Selection of optimal intensity measures for fragility assessment of circular tunnels in soft soil deposits

Zhong-Kai Huang[a,b], Kyriazis Pitilakis[b], Sotirios Argyroudis[d,b], Grigorios Tsinidis[c], Dong-Mei Zhang[a*]

[a]Key Laboratory of Geotechnical and Underground Engineering of Ministry of Education, Department of Geotechnical Engineering, Tongji University, Shanghai 200092, China

[b]Laboratory of Soil Dynamics and Geotechnical Earthquake Engineering, Department of Civil Engineering, Aristotle University, Thessaloniki, Greece

[c]VCE, Vienna Consulting Engineers ZT GmbH

[d]Department of Civil and Environmental Engineering, Brunel University London, UK

*Corresponding author: dmzhang@tongji.edu.cn

Abstract

This study aims to identify optimal intensity measures (*IMs*) for use in probabilistic seismic demand models (PSDMs) for circular tunnels in soft soil deposits. To this end, we performed an extended numerical parametric study involving two-dimensional time history analyses of selected soil-tunnel configurations to evaluate the response of the selected tunnels under transverse seismic shaking. A series of 18 *IM*s were selected and tested, corresponding to free field conditions. The selected *IM*s were tested on several metrics, such as correlation, efficiency, practicality, and proficiency, based on an extended number of regression analyses between the *IM*s and the damage measure (*DM*), for the studied tunnels. *DM* is defined as the ratio of the actual bending moment (*M*) to the capacitive bending moment (M_{Rd}) of the tunnel lining. The results indicate that the peak ground acceleration (*PGA*) at the ground surface can be considered as the optimal *IM* for the shallow tunnels, whereas the peak ground velocity (*PGV*) can be considered as the optimal *IM* for both the moderately deep and deep tunnels. Finally, various fragility curves were constructed for the studied circular tunnels under the context of PSDMs. The findings of this study can serve as a reference for the seismic fragility analysis of circular tunnels in soft soil deposits, toward more reliable quantitative risk analysis (QRA), improved resilience, and adaptability of transportation networks.

Keyword: *Seismic intensity measures; circular tunnels; probabilistic seismic demand model; fragility curve; soil-tunnel interaction*

1. Introduction

In recent decades, large-scale tunnel construction projects have been conducted worldwide to meet various public needs, particularly as part of transportation and utility networks in densely populated urban areas [1-3]. Observations of severe earthquakes that have occurred in the past have revealed that tunnels are typically less susceptible to damage and have better behaviour than above-ground structures [4, 5]. However, several cases of severe damage, and even collapse of tunnels and other underground structures, have been reported in the literature. The earthquake-induced damage and failure of Daikai Station in Japan in 1995 [6, 7], Bolu Tunnel in Turkey in 1999 [8, 9], and Longxi Tunnel in China in 2008 [10, 11] are representative examples, all of which resulted in significant losses [5, 12]. Considering the crucial role of tunnels in the transportation and utility networks of countries, regions, and cities, it is of paramount importance to investigate the seismic fragility and perform quantitative risk analysis of these structures [13, 14].

Fragility curves are commonly used to describe the conditional probability of a structure reaching or exceeding predefined damage states against a selected intensity measure (*IM*). The selection of appropriate *IMs* is one of the main prerequisites for reliable fragility and probabilistic seismic demand analyses [15, 16], and previous studies have recognised the importance of this prerequisite [17]. In particular, *IM* serves as an intermediate variable between seismic hazard analyses and structural demand assessments [18-20]. More importantly, an appropriate *IM* should be able to reflect the main characteristics of amplitude, frequency content, and duration of motions, reduce the variance of seismic structural performances, and accurately predict the responses of structures.

In recent decades, a variety of fragility curves has been proposed by different researchers for underground structures under different soil conditions, by using different *IMs*. Such fragility curves were originally based on expert elicitations [21] or damage data obtained from observations of previous earthquakes [23-25]. More recently, numerical approaches have been developed and applied to construct fragility curves for circular tunnels [25-31], rectangular tunnels [26, 32-34] and other underground structures [35-38]. A more detailed introduction of fragility curves for tunnels and other underground structures can also be found in Huang et al. [14] and Tsinidis et al. [3].

Most of the aforementioned fragility curves have been constructed in terms of various intensity measures, selected on the basis of expert judgment. In particular, the frequently selected *IMs* for tunnels include peak ground acceleration (*PGA*) [25], peak rock acceleration (*PRA*) [22], peak ground velocity (*PGV*) [14], permanent ground displacement (*PGD*) [24], and

Arias intensity (*AI*) [27]. The selection of these *IMs* has not been well-discussed or defended in most of the aforementioned studies. For practical reasons, *PGA* is the most commonly used *IM* for constructing fragility curves for tunnels. In contrast, some researchers [34, 36, 39] reported that *PGV* exhibits a better correlation with the seismic response of underground structures, in comparison with *PGA*, particularly in the case of deep tunnels. Therefore, there is no clear consensus as to which *IM* can be considered as the optimal *IM* for constructing analytical or empirical fragility curves of tunnels. Moreover, the optimal *IMs* used in the fragility analysis tend to vary significantly with local soil conditions, structure typologies, or even the seismic demand parameters used in the analysis [3]. This work aims to determine, for the first time in the literature, the optimal *IM* for constructing analytical or empirical fragility curves of tunnels by analysing 18 *IMs* commonly used in earthquake engineering and risk analysis of tunnel structures.

Several metrics have been proposed to identify optimal seismic *IMs* for structural evaluation, including efficiency, practicality, proficiency, sufficiency, and hazard computability [15, 16, 18, 40]. To date, these evaluation metrics and related works have focused on buildings [41-44], bridges [45, 46], and more recently, pipelines [47] and dams [48]. To the best of the authors' knowledge, there exists no relevant work dealing with tunnels.

The analytical framework of this paper is illustrated in Fig.1. First, we present a detailed description of the numerical modelling for the investigated tunnels. The proposed numerical framework takes into account the effects of soil-structure-interaction, local soil conditions, ground motion characteristics and tunnel burial depths. Then, the general concept of a probabilistic seismic demand model (PSDM) and an optimal *IM* are briefly introduced. Then, the selected 18 *IM*s are examined based on the calculated seismic responses of the tunnels using selection criteria, such as correlation, efficiency, practicality, and proficiency. Thorough analysis of the results leads to the identification of the optimal *IM*s for the PSDMs of the examined tunnel-soil configurations. Different fragility curves are established for the investigated systems in the context of PSDMs. The derived fragility curves are expected to be used within a critical infrastructure risk quantification framework, while the analysis of different *IMs* provides comprehensive insights into the selection of optimal *IMs* for the construction of fragility curves for underground structures.

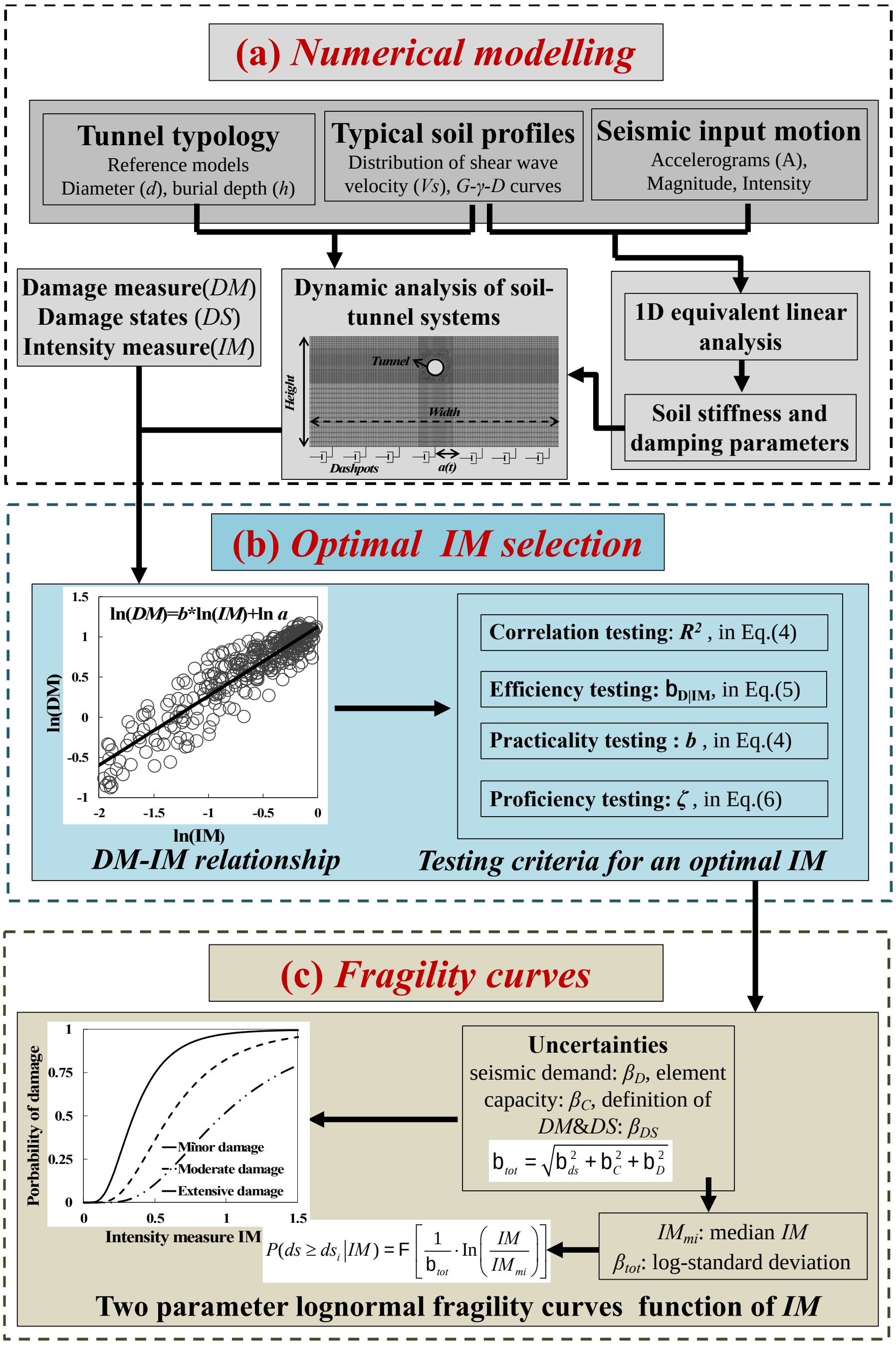

Fig.1 Schematic of the analytical framework for the fragility analysis of tunnels

2. Numerical model and analyses

2.1 Description of numerical model

A detailed two-dimensional (2D) numerical model of the soil-tunnel system was established using the general-purpose finite element software package ABAQUS [49], as depicted in Fig.2. The analysis was conducted under plane strain conditions.

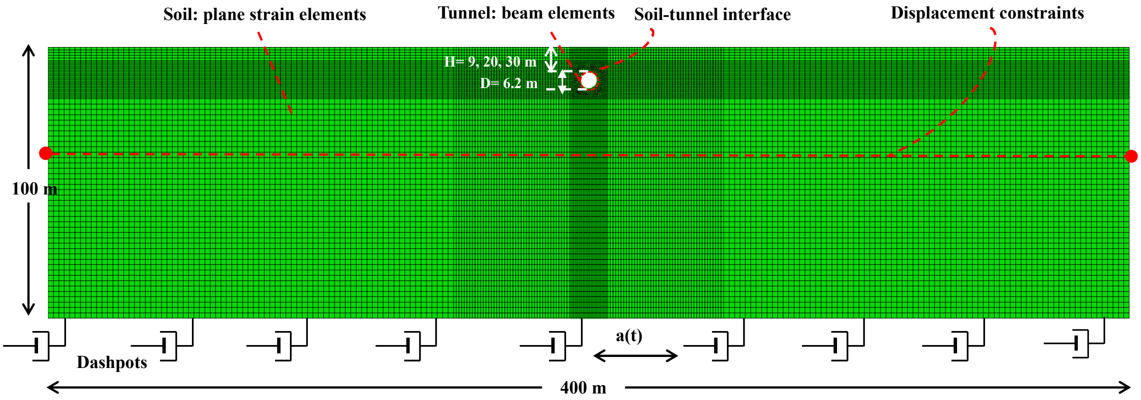

Fig.2 2D numerical model of the soil-tunnel system

We conducted a sensitivity analysis for various model dimensions to investigate the potential boundary effects and finally selected a soil grid with a width of 400 m to ensure 'free-field' conditions at the lateral boundary. The depth of the model was set at 100 m and elastic bedrock was used as the ground beyond this depth.

The tunnel lining was simulated using two-node beam elements, concerning the calculation efficiency. The type of beam elements used could model the lining forces and deformations well [36,49]. The soil was discretised using four-node quadratic reduction integral plane strain elements. A visco-elasto-plastic model with the Mohr-Coulomb yield criterion was adopted to simulate the soil's constitutive characteristics, as described below. A finer discretisation was adopted near the tunnel structure, as illustrated in Fig.2, to better capture the soil-tunnel interaction effects. The selected element size in the model satisfied the accuracy requirement for the dynamic analysis. It was found that a denser mesh size had a negligible effect on the final results, while the computational cost increased significantly.

The interface between the soil and tunnel lining was simulated using a finite-sliding hard contact algorithm [49]. The tangential behaviour of the interface followed the penalty algorithm with a friction coefficient of μ = 0.6, corresponding to a friction angle of 31° for the soil-tunnel interface. As for the normal interface behaviour, a hard contact formulation was adopted to enable the potential separation of the lining and surrounding soil elements and transfer of tensile stresses to the soil element. The interface simulation approach described above has been commonly used by other researchers in similar studies [31, 36, 50].

The base boundary was modelled as an elastic bedrock, by introducing proper dashpots, in accordance with the scheme proposed by Lysmer and Kuhlemeyer [51]. The selected acceleration time histories were imposed through the aforementioned dashpots in the horizontal direction, to assure 'quasi transparent' conditions, as shown in Fig.2. The dashpot coefficient C is defined by Eq. (1), as follows:

$$C = \rho_b \times V_{sb} \times A \quad (1)$$

where ρ_b and V_{sb} are the mass density and shear wave velocity of the underlying elastic bedrock, corresponding to 2.1 t/m^3 and 500 m/s, respectively. A is the 'effect area' of each dashpot and is determined by the horizontal element size at the base of the numerical model. Additionally, horizontal kinematic constraints were imposed on the nodes at the two lateral boundaries of the model, forcing the opposite vertical sides of the numerical model to exhibit the same horizontal movement.

With regard to the simulation of the nonlinear soil response, 1D soil seismic response analyses were first performed using the numerical code EERA [52], to obtain the strain-compatible shear modulus G gradients of soil profiles along the depth of the model. The adopted modelling method for calculating the equivalent soil stiffness is recommended in the relevant FHWA guidelines [53] for seismic analysis of tunnels. The estimated soil properties were integrated with a Mohr–Coulomb yield criterion in the 2D soil-tunnel analysis, to account for the soil response under higher strains. The soil modelling approach described above has been extensively validated against experimental results and predictions of other numerical models; for example, please refer to [54, 55].

Previous studies have highlighted the importance of damping on the seismic response of underground structures [56]. In this study, two types of damping were considered: hysteretic damping induced by the soil constitutive model used during elasto-plastic analyses and frequency-based viscous damping. The latter was modelled in terms of the Rayleigh type and ranged from 2% to 8%, based on results of the 1D soil response analyses performed for the selected soil deposits. The commonly adopted double frequency calibration method [26, 56] was utilised to determine the Rayleigh coefficients.

Each numerical analysis was performed in two steps. The first step aimed to apply the gravity load and, thus, establish the geostatic stress field in the model. In this step, the base boundary of the numerical model was fixed both in the horizontal and vertical directions. Subsequently, an implicit dynamic step was conducted wherein the dynamic load was applied uniformly over the dashpots and the base boundary in the horizontal direction in terms of an acceleration time history. In general, the specific tunnel excavation process can be expected to change the initial state of geostatic stresses around the tunnel [9], thus affecting the seismic response of the tunnel lining to a certain degree. However, in this study, we simply applied the geostatic stresses on the entire model and consequently, to the tunnel lining as well, to produce a reasonable "reference" initial stress state of the ground, because the main focus of the study is the dynamic inelastic response of the soil. This simplified modelling method has proven to be reasonably accurate and has also been used in previous works by Argyroudis et al. [26], Hatzigeorgiou and Beskos [4], de Silva et al. [30], Hu et al. [31] and Huh et al. [33].

The main numerical analyses were used to calculate the lining forces to compute the *DM* and to determine the optimal *IM* for the corresponding fragility curves. Moreover, the results of the analyses were used to compute the ground motion at the ground surface under 'free-field' conditions, i.e., away from the tunnel and the boundaries of the model. The time history motion of the latter was used to define the values of the examined *IMs*.

All the numerical simulations presented below were conducted under total stresses assuming undrained conditions. This assumption is in line with previous studies [14, 26, 58]. The potential development of excess pore water pressures during strong shaking, and the phenomena associated with it, are beyond the scope of this study.

2.2 Soil-tunnel configurations

The properties of the examined soil profiles, denoted as soil deposits D1, D2, and D3 herein, were selected based on the stratigraphy of the real metro tunnels in Shanghai, China. The profiles above correspond to soil type D according to EC8 [59], or equivalently ground type III or IV according to the Chinese seismic design code [60]. In all the soil profiles used in this work, we adopted the same depth of 100 m for the 'seismic bedrock' where the input motions were applied. It is actually the underlying stiff ground (such as soil type B of EC8 or soil class II of the Chinese seismic design code) with an average shear wave velocity of 500 m/s or higher. In Shanghai City, the real bedrock, with V_s > 1000 m/s, is found at greater depths (i.e. > 400 m). The selected depth of 100 m satisfies the requirement for limited boundary effects on the computed response of the tunnels, while keeping the dimensions of the numerical models ‘bounded’ to allow for reasonable computational times. Fig.3 illustrates the main soil properties, including shear wave velocities V_s, density ρ, cohesion c, and friction angle φ, for the examined soil deposits, derived based on site investigations and laboratory tests. Additionally, the nonlinear behaviour of the selected soil profiles under ground shaking is described by virtue of the G/G_{max}-γ-D(%) curves, as illustrated in Fig.4, following the code for the seismic design of underground structures in Shanghai [61].

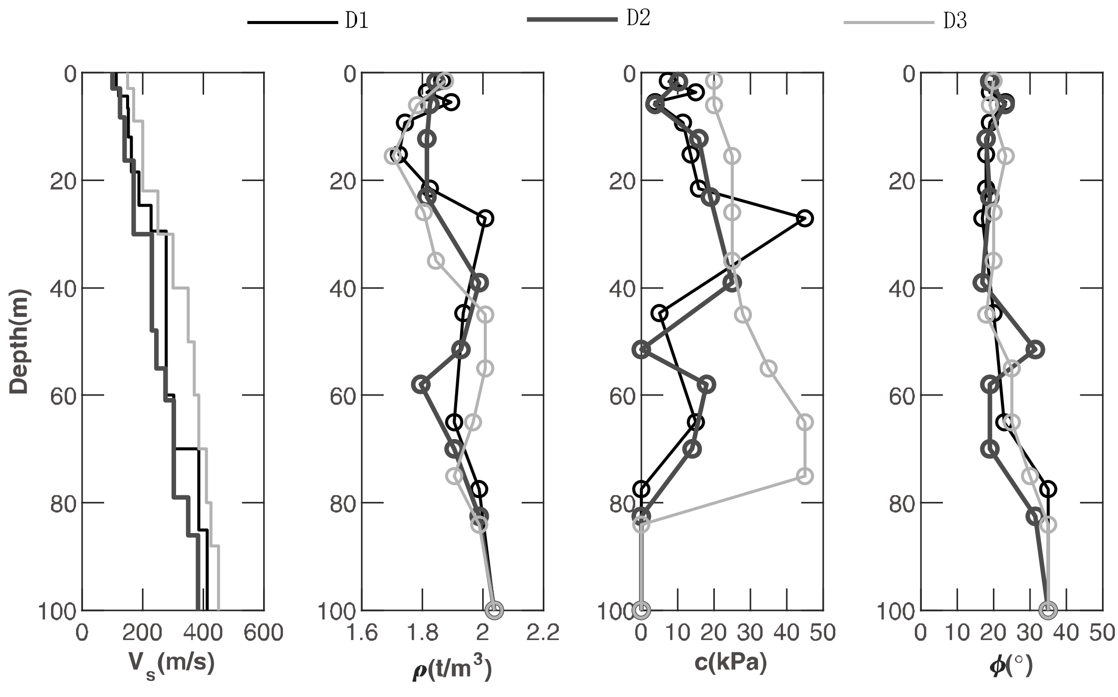

Fig.3. Soil properties for the examined soil deposits

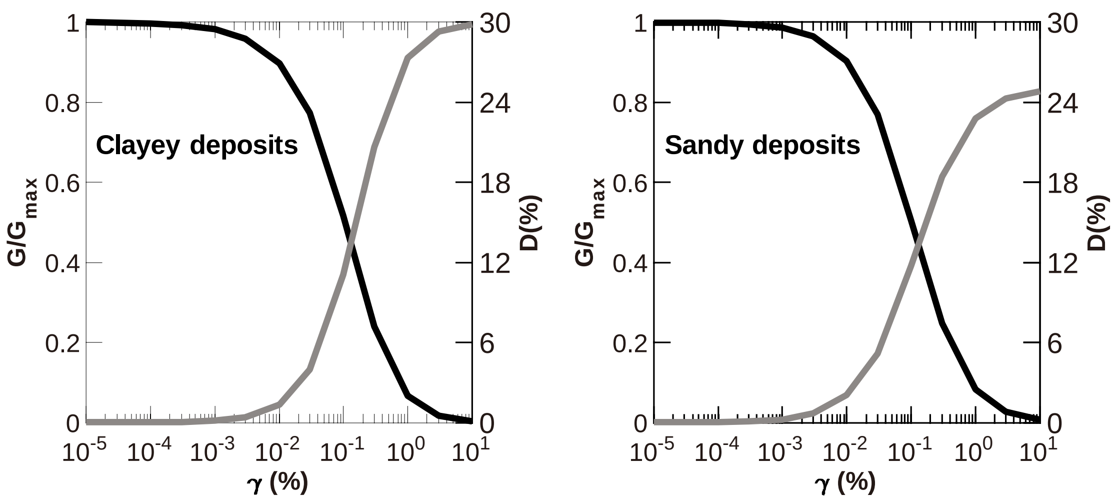

Fig.4. Adopted G-γ-D curves for clayey and sandy deposits

A typical circular tunnel cross-section, commonly found in the Shanghai metro system of China, was considered in this study. The lining ring has an outer diameter D_o of 6.2 m and is 0.35 m thick. The detailed properties of the investigated tunnel are summarised in Table 1. The burial depth h of the investigated tunnel ranges between 9, 20, and 30 m, to account for shallow, moderately deep, and deep tunnel sections, respectively. Hence, the overburden depth ratios (defined as h/D_o) vary between 1.45 and 4.84.

Table 1. Physical and mechanical properties of the examined tunnels

Parameters	Typical values
Burial depth, h (m)	9.0, 20.0, 30.0
Bending reinforcement, A_s (cm^2/m)	21.0, 43.0, 58.0
Tunnel external diameter, D_o (m)	3.1
Lining wall thickness, t (m)	0.35
Concrete elastic modulus, E_c (Gpa)	3.55
Concrete Poisson ratio, v_c	0.2
Steel elastic modulus, E_s (Gpa)	200
Steel Poisson ratio, v_s	0.2

Concrete cover depth of lining, c_s (cm)	5.0

2.3 Ground motions

Selection of ground motions is vital for the seismic vulnerability analysis of structural elements or systems at risk. In this study, the most commonly used spectral matching method [62] was adopted to conduct the selection of the seismic records. The selection satisfied the following three criteria: (1) 5.0 < moment magnitude M_w < 8.0, (2) 1 km < epicentral distance R < 80 km and (3) 0.1 < PGA < 0.8. A suite of 12 ground motions was finally selected to cover the variability of the intensity [63] and frequency characteristics of the seismic waves. Various approaches may be found in the literature to examine the relationship between a numerically predicted engineering demand parameter *EDP* and a selected seismic *IM*, i.e. the incremental dynamic analysis (IDA), multiple-stripe analysis, and cloud analysis. In this study, the first method, i.e. IDA, was employed because with this approach, a wide range of ground motion amplitudes may be covered; hence, the effect of an increment in seismic intensity on the seismic response of the tunnel lining may be thoroughly evaluated. In general, the number of ground motions required for IDA [57] is dependent on the research objectives and structural properties. Previous research [63] indicated that a series of 10 to 20 real ground motion records can adequately capture the epistemic uncertainty in ground motion and provide sufficient accuracy for the calculation of seismic demands. Hence, in this study, a suite of 12 ground motions was selected and the *PGA* value for each ground motion was scaled from 0.1 g to 1.0 g, to evaluate the effect of the increment of seismic intensity on the seismic response of the tunnel lining. All ground motions were selected from the PEER strong earthquake record database [64]. The selected ground motions were recorded under soil conditions with Vs_{30} higher than 380 m/s, similar to those of soil type B of EC8 [59] or soil class II of the Chinese seismic design code [60]. We selected appropriate ground motions representative of soil type B, because the assumed seismic bedrock, where the records were applied in the numerical models, was considered at a depth of 100 m with a V_s = 500 m/s. Hence, the records from sites similar to the underlying stiff ground of Shanghai soil conditions were adopted in this work. Table 2 lists the basic information regarding the selected ground motions, while Fig.5 depicts the comparison of the acceleration response spectra of the 12 unscaled ground motions with the design response spectrum from the Chinese seismic design code [60]. As shown in Fig.5, the average spectrum of the selected earthquake matches well with the design spectrum. In the numerical analyses, each selected record was scaled from 0.1 g to 1.0 g with a gradient of 0.1 g in accordance with IDA [57], to obtain the structural response of the tunnel lining under a gradually increasing intensity of ground motion. Thus, a total of 120 input motions were used to develop the fragility curve.

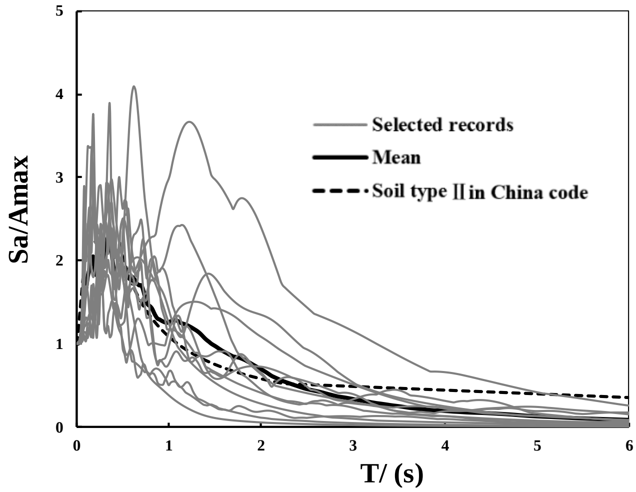

Fig.5. Acceleration response spectra of the selected records

Table 2. Selected records used in this study

No.	Earthquake	Station name	Time	Mag. (M_w)	R (km)	PGA (g)
1	Superstition Hills-01	Imperial Valley W.L. Array	1987	6.22	17.59	0.13
2	Parkfield-02_ CA	Parkfield-Cholame 2WA	2004	6.00	1.63	0.62
3	Tottori_ Japan	TTR008	2000	6.61	6.86	0.39
4	Kobe_ Japan	Port Island	1995	6.9	3.31	0.32
5	Imperial Valley-07	El Centro Array #11	1979	5.01	13.61	0.19
6	Loma Prieta	Treasure Island	1989	6.93	77.32	0.16
7	Kern County	Taft Lincoln School	1952	7.36	38.42	0.15
8	Parkfield	Cholame-Shandon Array	1966	6.19	12.9	0.24

9	Borrego Mtn	El Centro Array #9	1968	6.63	45.12	0.16
10	San Fernando	Castaic - Old Ridge Route	1971	6.61	19.33	0.34
11	Northridge-01	LA - Hollywood Stor FF	1994	6.69	19.73	0.23
12	Imperial Valley-02	El Centro Array #9	1940	6.95	6.09	0.28

2.4 Representative numerical results

Representative numerical results are presented as follows. Fig.6(a)–(c) depict the time series of the dynamic bending moment at a critical location (θ = 45°) for all three tunnel cases in soil type D3, under the excitation of EQ2 with intensities of 0.10 g and 1.0 g, respectively. For all three tunnel cases, the dynamic bending moment typically increases as the intensity increases. In particular, for a low intensity of 0.10 g, the dynamic bending moment is small, oscillating typically around 0 kN·m/m. For a high intensity of 1.00 g, three typical stages are observed for the evolution of the dynamic bending moments, including a transient stage, steady-state stage, and post-earthquake residual stage. Considering the results from the shallow tunnel as an example, presented in Fig.6 (a), the dynamic bending moment increases significantly to a high value of 536 kN·m/m after few cycles, and then oscillates around a mean residual value, and finally, a permanent residual bending moment of 264 kN·m/m is observed at the end of the earthquake loading. The observed residual bending moment is due to the effects of stress redistribution of the soil around the tunnel, caused by potential nonlinear behaviour of the soil-tunnel interface and soil yielding.

Further results and discussion on the evolution of the dynamic bending moments at the critical sections of the tunnel lining, dynamic soil plastic strain distributions in the vicinity of the tunnel, as well as typical total bending moment distributions computed along the tunnel perimeter can be found in the authors' previous work, i.e. in [14].

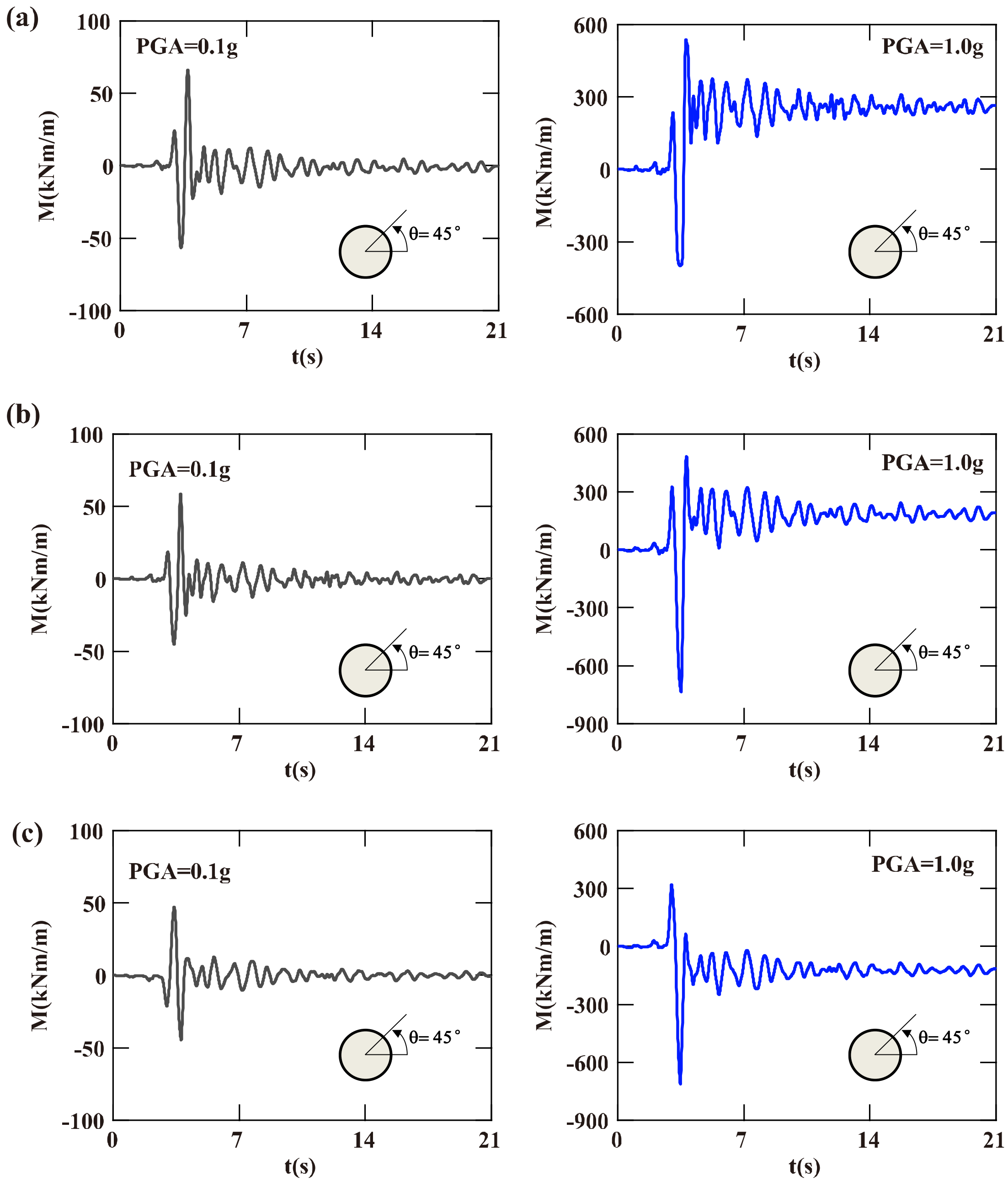

Fig.6. Bending moment time histories computed for EQ2 at a crucial lining section (θ = 45°) of the tunnel located in soil type D3: (a) shallow tunnel, (b) moderately deep tunnel, and (c) deep tunnel cases

3. Selection of optimal intensity measures (IMs)

3.1 Definition of damage states

An important step in the definition of fragility curves of any element at risk is the selection of adequate damage measures (*DMs*) [13]. The definition of damage states, based on the *DM*, constitutes the subsequent step in the definition of a PSDM and, thus, in the assessment of seismic vulnerability. To date, there are few relevant damage measures for tunnels, in comparison with those for above ground civil infrastructure, i.e. bridges and buildings. The few damage measures that have been proposed and successfully applied in the vulnerability analysis of tunnels may be typically classified into two types: force-based *DMs* [25-30] and displacement-based *DMs* [37]. For example, one of the first proposed *DMs* by Argyroudis and Pitilakis [25] is defined as the ratio of the actual bending moment to the capacity bending moment of the tunnel cross-section. Nguyen et al. [34] considered a *DM* defined as the ratio of the elastic bending moment to the yield moment at the critical sections of the tunnel frames. More recently, Andreotti and Lai [37] used a *DM* calculated as the relative displacement between the crown of the arch and the inverted arch divided by the equivalent diameter of the tunnel lining cross-section. A term defined as the ratio between the actual ratio e ($e=M/N$) and the capacity $(e)_{Rd}$ may be also considered as a potential *DM* in future work, where e is defined as the eccentricity of the actual axial force N of the tunnel lining cross-section and defined as the ratio of the actual bending moment M to the actual axial force N. However, further work is deemed necessary to determine different e/e_{Rd} limits for the corresponding damage states, namely no damage, minor damage, moderate damage, extensive damage, and collapse. This work, similar to one conducted by Du et al. [38], is certainly interesting but beyond the scope of this study. In general, the selection of the optimal *DM* is among the main research challenges in the risk assessment of structures; thus, it should be among the priorities of future research on the vulnerability assessment of underground structures, such as tunnels. To this end, a widely used *DM* proposed in similar research works [e.g. 25-28] was considered in this study, leaving the comparative research of other *DMs* as a future endeavour. This *DM* is defined as the ratio of the actual bending moment (M) to the capacity (M_{Rd}) bending moment of the tunnel cross-section. Herein, the actual bending moment (M) is obtained from the full dynamic time history analysis, whereas the capacity bending moment (M_{Rd}) is computed based on the material properties and geometric characteristics of the tunnel cross-section. Five different damage states are determined, including no damage, minor damage, moderate damage, extensive damage, and collapse, as listed in Table 3.

Table 3. Definition of damages states [25]

Damage state (ds_i)	ds_0, no	ds_1, minor	ds_2, moderate	ds_3, extensive	ds_4, collapse

	damage	damage	damage	damage	
Range of *DM*	$M_{sd}/M_{Rd} \leq$ 1.0	$1.0 < M_{sd}/M_{Rd} \leq 1.5$	$1.5 < M_{sd}/M_{Rd} \leq 2.5$	$2.5 < M_{sd}/M_{Rd} \leq 3.5$	$M_{sd}/M_{Rd} \geq$ 3.5
Central value of *DM*	-	1.25	2.00	3.00	-

3.2 Selection of examined seismic intensity measures

The seismic response of the soil-tunnel system is considerably complex, and this complexity can affect the accuracy and efficiency of numerically derived fragility curves. Consequently, it is essential to examine a wide range of potential *IMs* and identify the optimal *IM* for predicting the seismic response of the tunnel. The effect of the optimal *IM* on the fragility curves should subsequently be verified. In this study, 18 commonly used *IMs* were considered for the development of the PSDMs (Table 4). More information on the selected seismic *IMs* can be found elsewhere, e.g. see references in the last column of Table 4.

Table 4. Intensity measures used in analysis

No.	*IMs* (units)	Notation	Reference
1	Peak Ground Acceleration (g)	*PGA*	Kramer [64]
2	Peak Ground Velocity (m/s)	*PGV*	Kramer [64]
3	Peak Ground Displacement (m)	*PGD*	Kramer [64]
4	*PGV*/*PGA* (s)	*FR1*	Kramer [64]
5	Acceleration Root-Mean-Square *RMS* (g)	A_{rms}	Housner and Jennings [65]
6	Velocity *RMS* (cm/s)	V_{rms}	Housner and Jennings [65]
7	Displacement *RMS* (m)	D_{rms}	Housner and Jennings [65]
8	Arias Intensity (m/s)	I_A	Arias [66]
9	Characteristic Intensity (-)	*Ic*	Park et al. [67]
10	Specific Energy Density (cm^2/s)	*SED*	-
11	Cumulative Absolute Velocity (cm/s)	*CAV*	Kramer [64]

12	Acceleration Spectrum Intensity (g*s)	*ASI*	Housner [17]
13	Velocity Spectrum Intensity (cm)	*VSI*	Housner [17]
14	Housner Intensity (m)	*HI*	Housner [17]
15	Sustained Maximum Acceleration (g)	*SMA*	Nuttli [68]
16	Sustained Maximum Velocity (cm/s)	*SMV*	Nuttli [68]
17	Effective Design Acceleration (g)	*EDA*	Benjamin [69]
18	A95 Parameter (g)	*A95*	Sarma and Yang [70]

3.3 Overview of PSDM

PSDM provides a relationship between an engineering demand parameter *EDP*, which describes the response of the structure or system under study, and the seismic *IM*. A lognormal distribution is commonly used to describe such a relationship [71-75], as given in Eq.(2) below:

$$p[EDP \geq edp \,|\, \mathrm{IM}] = 1 - \Phi\left(\frac{\ln(edp) - \ln(S_{EDP|IM})}{\beta_{\mathrm{D|IM}}}\right) \tag{2}$$

where *edp* or *EDP* is the peak engineering demand, $\Phi(\bullet)$ is the standard normal cumulative distribution function, $S_{EDP/IM}$ is the median demand with respect to a seismic hazard *IM*, whereas $\beta_{D|IM}$ is the logarithmic standard deviation of the demand conditioned on the *IM*. Furthermore, the relationship between the structural demand $S_{EDP/IM}$ and *IM* can be given in the power-law function, as indicated in Eq.(3):

$$S_{EDP|IM} = a\,\mathrm{IM}^{b} \tag{3}$$

where *a* and *b* are the coefficients of the regression. Eq.(3) can also be redefined as in Eq.(4), which describes a linear expression of the natural logarithms of the demand $S_{EDP/IM}$ and the *IM*:

$$\ln(S_{EDP|IM}) = b \cdot \ln(\mathrm{IM}) + \ln a \tag{4}$$

The uncertainty in the seismic demand $\beta_{\mathrm{D|IM}}$ is approximated as the dispersion of the simulated demand with respect to the regression fit for the calculated damage data obtained from the non-linear time history analyses, as shown in Eq.(5):

$$\beta_{\mathrm{D|IM}} \cong \sqrt{\frac{\Sigma(\ln(edp_i) - \ln(S_{EDP|IM}))^2}{N-2}} \qquad (5)$$

IMs have a significant impact on the uncertainty associated with the derived fragility curves of the element at risk, and hence, an optimal *IM* should be able to reflect the most accurate correlation between the structural response and the *IM*. In this study, four different criteria were examined for determining the optimal *IMs* for tunnels, namely correlation [20], efficiency [16], practicality [18], and proficiency [16]. The selected metrics and the corresponding testing results of the examined *IMs* for the shallow, moderately deep, and deep tunnel cases are presented and discussed below.

3.4 Results of PSDM study

3.4.1 Correlation testing

The correlation criterion indicates how well the regression model of Eq.(4) fits the calculated seismic demand. This criterion is known as the correlation coefficient R^2 and ranges from 0 to 1. A higher R^2 indicates less scattering and a better correlation relationship between *DM* and *IM*. Correlation testing of the examined *IMs* is based on the results of linear regression analyses between the natural logarithm of the intensity measure ln*IM* and the damage measure ln*DM* (i.e. Eq.(4)). Representative examples of regression analyses for four selected *IMs* are provided in Fig.7. The regressions refer to the results obtained from the shallow tunnel cases, as listed in Table 4, namely *PGA*, *PGV*, *PGD*, and *FR1*. The estimated regression parameters for all the examined *IMs* are summarised in Table 5 for the shallow tunnel case.

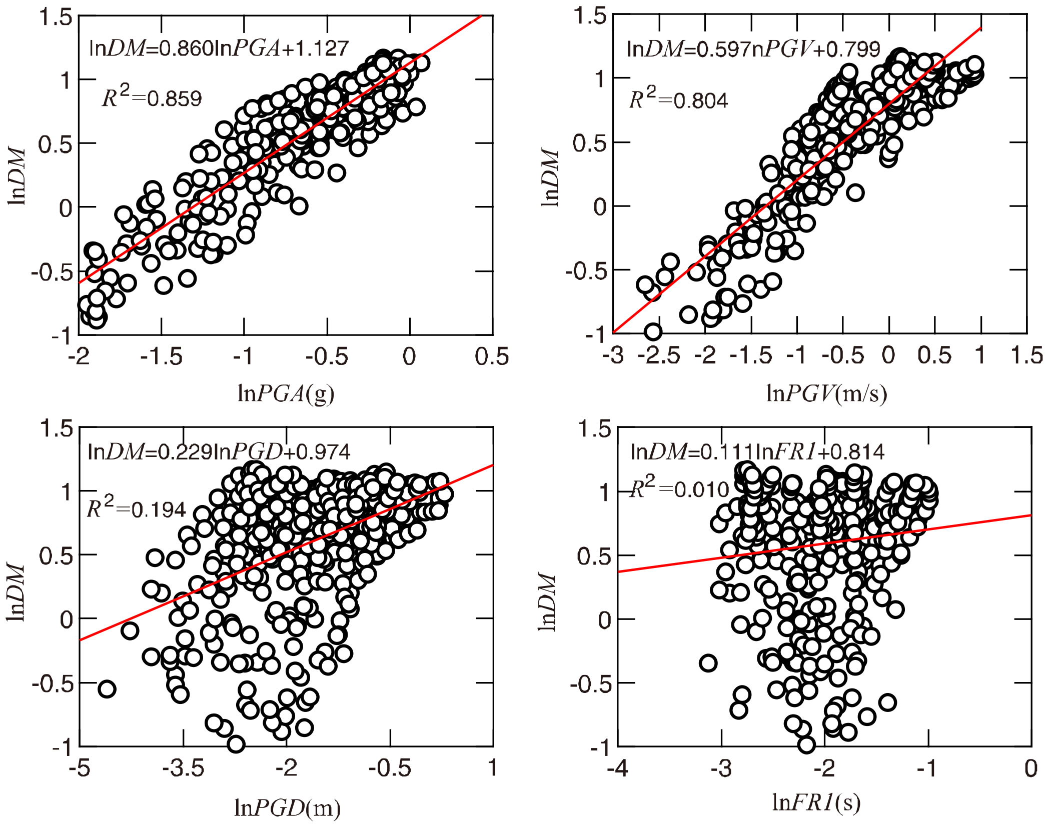

Fig.7. Regression analyses between four representative seismic *IMs* and *DM* (shallow tunnel)

Table 5. All regression parameters for shallow tunnels

IM	Parameter *b*	Parameter *a*	Correlation coefficient (R^2)
PGA	0.860	3.086	0.859

PGV	0.597	2.223	0.804
PGD	0.229	2.649	0.194
FR1	0.111	2.257	0.010
A_{rms}	0.603	7.729	0.643
V_{rms}	0.422	0.618	0.438
D_{rms}	0.196	3.168	0.162
I_a	0.259	1.201	0.527
I_c	0.376	3.536	0.583
SED	0.160	0.444	0.318
CAV	0.324	0.155	0.341
ASI	0.655	2.965	0.668
VSI	0.416	0.168	0.397
HI	0.348	0.257	0.335
SMA	0.450	2.872	0.434
SMV	0.332	0.507	0.34
EDA	0.760	2.945	0.647
A95	0.758	2.977	0.644

An optimal *IM* is characterised by a higher value of the correlation coefficient R^2. Figs.8, 9, and 10 summarise the calculated correlation coefficients R^2 for the considered *DM* with regard to the 18 *IMs* listed in Table 4 for the shallow, moderately deep, and deep tunnel cases, respectively. It can be observed (Fig.8) that *PGA* has the strongest correlation with the *DM* for the shallow tunnel cases, followed by *PGV* and *ASI*. The correlation coefficients R^2 for the three most correlated *IMs* are 0.859, 0.804, and 0.668, respectively. Furthermore, the weakest correlation between *IM* and *DM* is *FR*1 with a correlation coefficient of 0.010, followed by D_{rms} and *PGD* (i.e. correlation coefficients of 0.162

and 0.193, respectively).

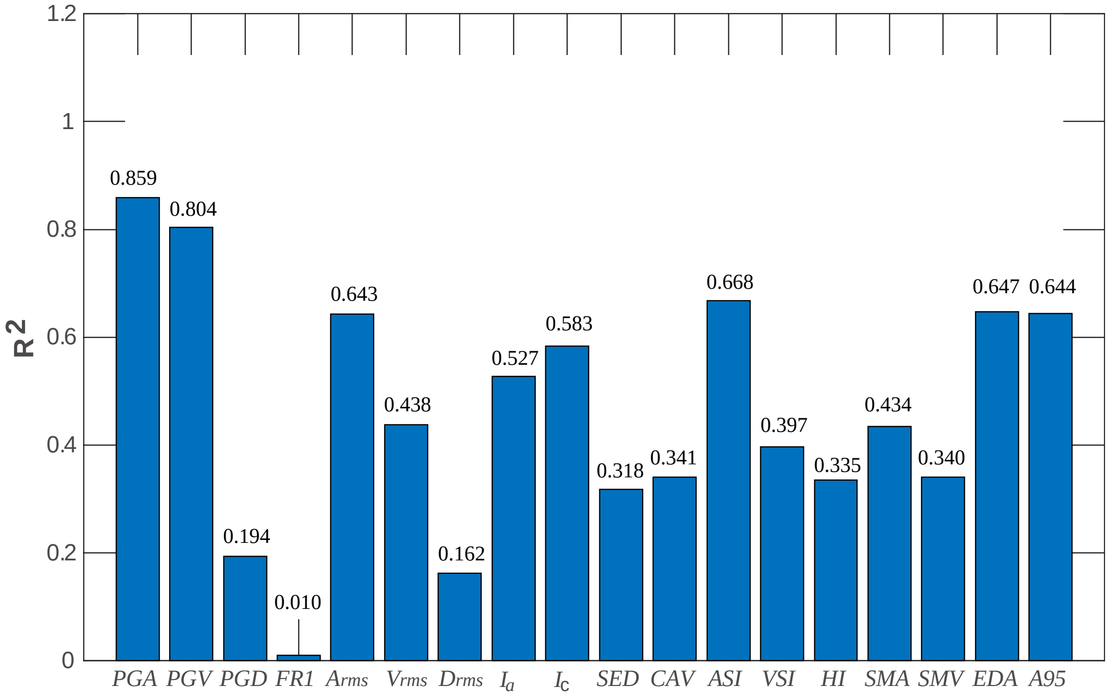

Fig.8. Regression parameter R^2 for the 18 tested *IMs* based on the numerical analyses of the shallow tunnel cases

For moderately deep tunnels, *PGV* tends to correlate most strongly with *IM* and *DM*, and the three most strongly correlated *IMs* are *PGV* > *VSI* > *HI* (see Fig.9). Their corresponding correlation coefficients are 0.922, 0.883, and 0.835, respectively. Moreover, *FR*1 tends to be the least correlated *IM*, as it has the lowest correlation coefficient of 0.410. Interestingly, this finding is well in line with the results of the shallow tunnel cases, indicating that *FR*1 demonstrates the weakest correlation for both the shallow and moderately deep tunnel cases. The second and third weakest correlated *IMs* are *ASI* and D_{rms}, with correlation coefficients of 0.457 and 0.528, respectively.

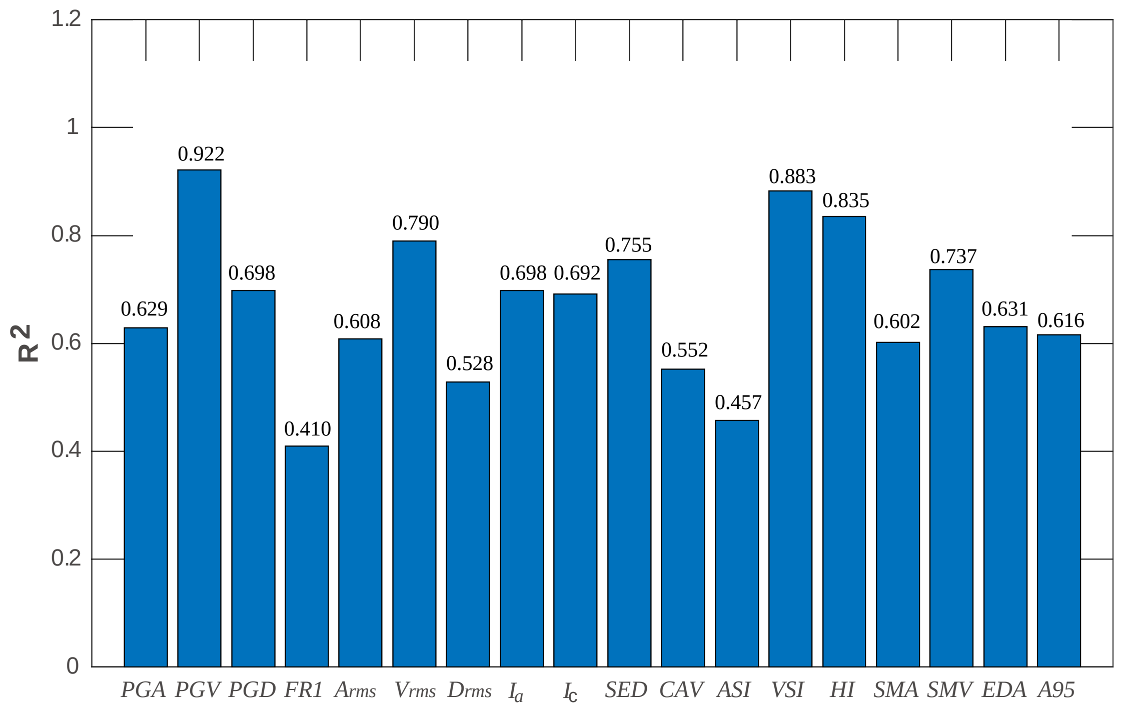

Fig.9. Regression parameter R^2 for the 18 tested *IMs* based on the numerical analyses of the moderately deep tunnel cases

Fig.10 depicts the computed results of the correlation coefficients for the deep tunnel cases. It can be demonstrated that *PGV* is again the most correlated *IM* in comparison with the other examined *IMs*; this finding holds true for the moderately deep tunnel cases as well, as discussed above. *VSI* and *HI* are two of the other highly correlated *IMs*. The correlation coefficients for the three most highly correlated parameters are 0.892, 0.864 and 0.837, respectively, whereas the lowest correlated *IM* with *DM* is *ASI*, followed by *FR*1 and A95. Their corresponding correlation coefficients are 0.401, 0.432, and 0.541, respectively.

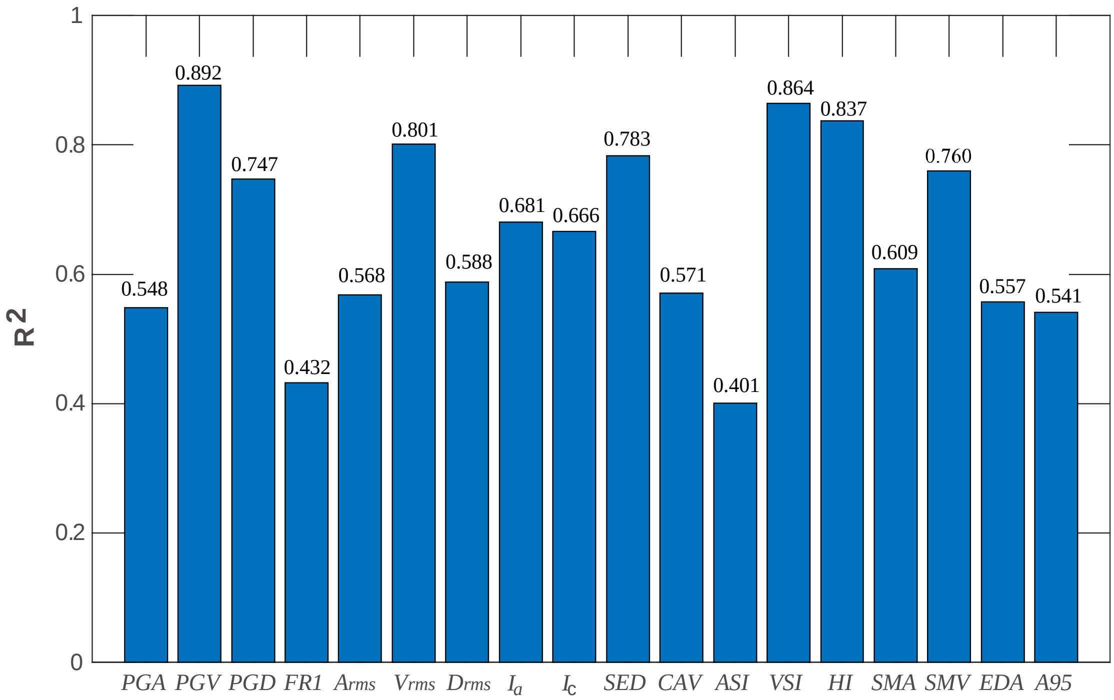

Fig.10. Regression parameter R^2 for the 18 tested *IMs* based on the numerical analyses of the deep tunnel cases

3.4.2 Efficiency testing

Efficiency is the most readily examined criterion for selecting an optimal *IM*. A more efficient *IM* leads to less variation in demand estimations for different values of the considered *IM*. In particular, in this study, an efficient *IM* is the one that provides the lowest value of standard deviation $\beta_{D|IM}$, as shown in Eq.(5).

The results of the efficiency analyses are depicted in Fig.11–13 for the shallow, moderately deep, and deep tunnel cases, respectively. For the shallow tunnels, *PGA*, *PGV*, and *ASI* are considered more efficient measures since they have smaller standard deviations $\beta_{D/IM}$ (Fig.11). Among them, *PGA* is the most efficient *IM* with the lowest standard deviation $\beta_{D/IM}$, i.e. 0.186. The corresponding $\beta_{D/IM}$ for the next two most efficient *IMs* are 0.219 and 0.285, respectively, which are slightly higher than that for *PGA*. The maximum standard deviation $\beta_{\mathrm{D/IM}}$ is observed for *FR*1, i.e. 0.492, indicating that this measure is the least efficient. This is followed by D_{rms} and *PGD*. Their corresponding standard deviations $\beta_{\mathrm{D/IM}}$ are 0.453 and 0.444, respectively, which are slightly lower than that for *FR*1.

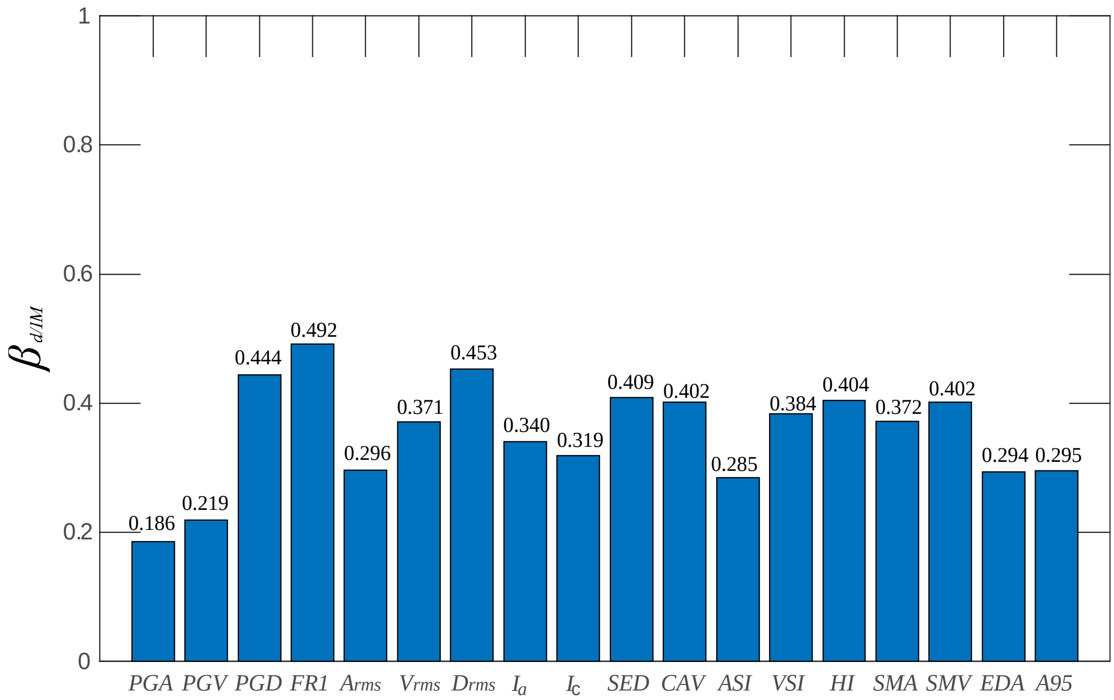

Fig.11. Regression parameter $\beta_{\mathrm{D/IM}}$ for the 18 tested *IMs* based on the numerical analyses of the shallow tunnel cases

Fig.12 shows the computed standard deviations $\beta_{\mathrm{D/IM}}$ for moderately deep tunnel cases. It can be observed that *PGV* is the most efficient *IM* with the smallest standard deviation of 0.135, followed by *VSI* and *HI* among the tested *IMs*. The values of $\beta_{\mathrm{D/IM}}$ for the latter *IMs* are 0.164 and 0.196, respectively. *FR*1 proves to be the least efficient *IM*, followed by *ASI* and D_{rms}. Their corresponding standard deviations are 0.369, 0.355, and 0.331, respectively.

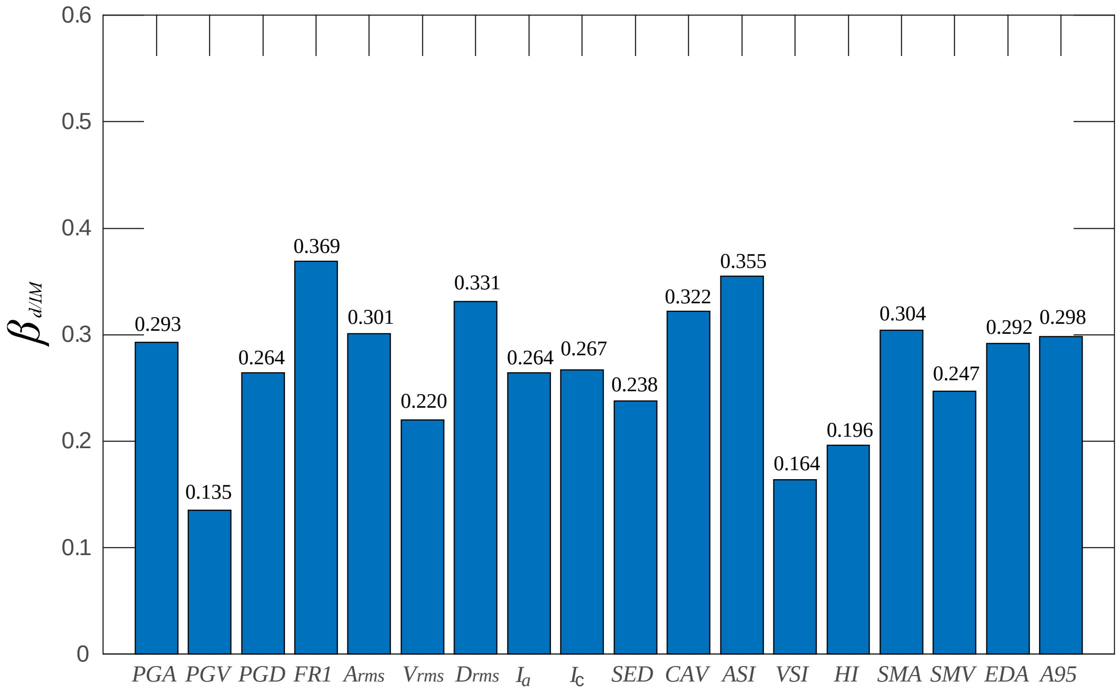

Fig.12. Regression parameter $\beta_{D/IM}$ for the 18 tested *IMs* based on the numerical analyses of the moderately deep tunnel cases

For the deep tunnel cases, *PGV* proves to be the most efficient *IM*, and the three best correlated *IMs* are *PGV* > *VSI* > *HI* (Fig.13). Interestingly, the above observation is also reported for the moderately deep tunnel cases. Their corresponding $\beta_{D/IM}$ values are 0.173, 0.195, and 0.213, respectively. In contrast, *ASI* exhibits the worst efficiency with the largest standard deviation of 0.408 among the tested *IMs*. *FR*1 and A95 are the other two least efficient *IMs* with slightly lower standard deviations, i.e. 0.398 and 0.357, respectively.

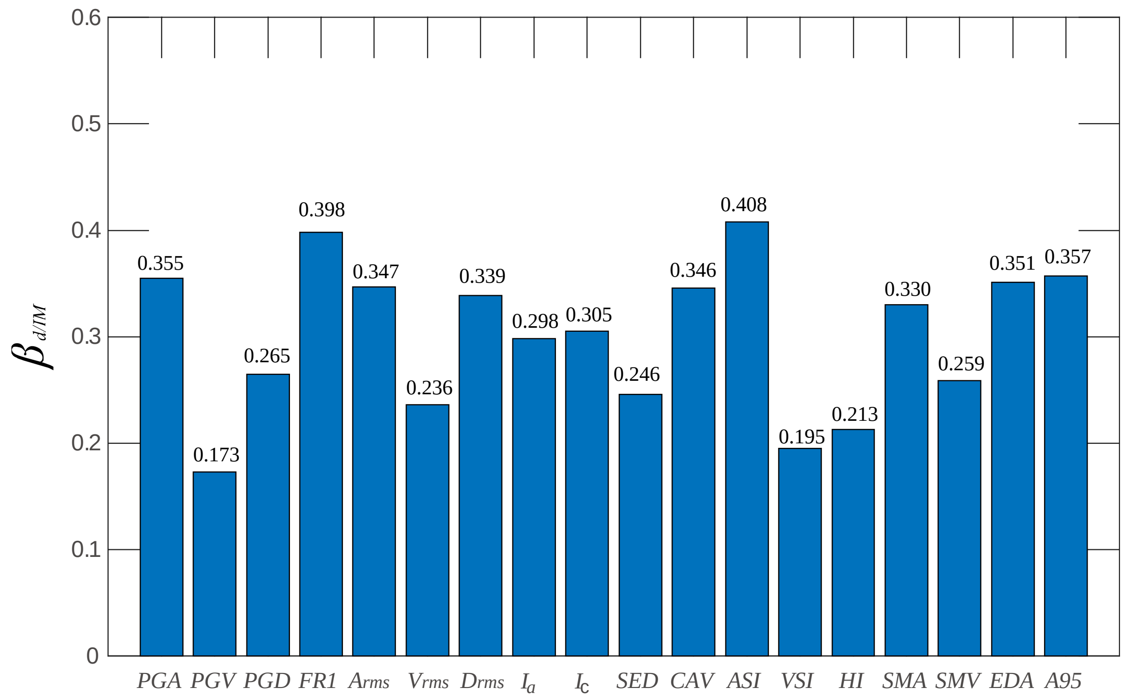

Fig.13. Regression parameter $\beta_{D/IM}$ for the 18 tested *IMs* based on the numerical analyses of the deep tunnel cases

3.4.3 Practicality testing

Practicality refers to the dependence of the structural response demand on the *IM*, and is represented by the regression parameter *b* in Eq.(4). A larger *b* indicates that the corresponding *IM* is more practical, since the structural response demand has higher dependence on the *IM*. Similarly, a smaller value of *b* indicates that the examined *IM* is less practical. If the value of *b* is close to zero, it implies that there exists no correlation between the structural response demand and *IM*.

Figs.14–16 summarise the *b* values calculated from the regression models for each *IM-DM* pair, for the shallow, moderately deep, and deep tunnel cases, respectively. For shallow tunnels, the comparisons in Fig.14

suggest that *PGA* is the most practical *IM* among others, because it has the maximum slope *b* of 0.86. *EDA* and A95 proved to be the second and third most practical *IMs*, with the corresponding slope *b* equal to 0.76 and 0.758, respectively. In contrast, *FR*1 is found to be the least practical *IM* among the other tested *IMs*, as it exhibits the minimum slope *b* of 0.111 for the examined cases. *SED* and D_{rms} prove to be the other two least practical *IMs*, with slightly higher slope values *b*, i.e. 0.160 and 0.196, respectively.

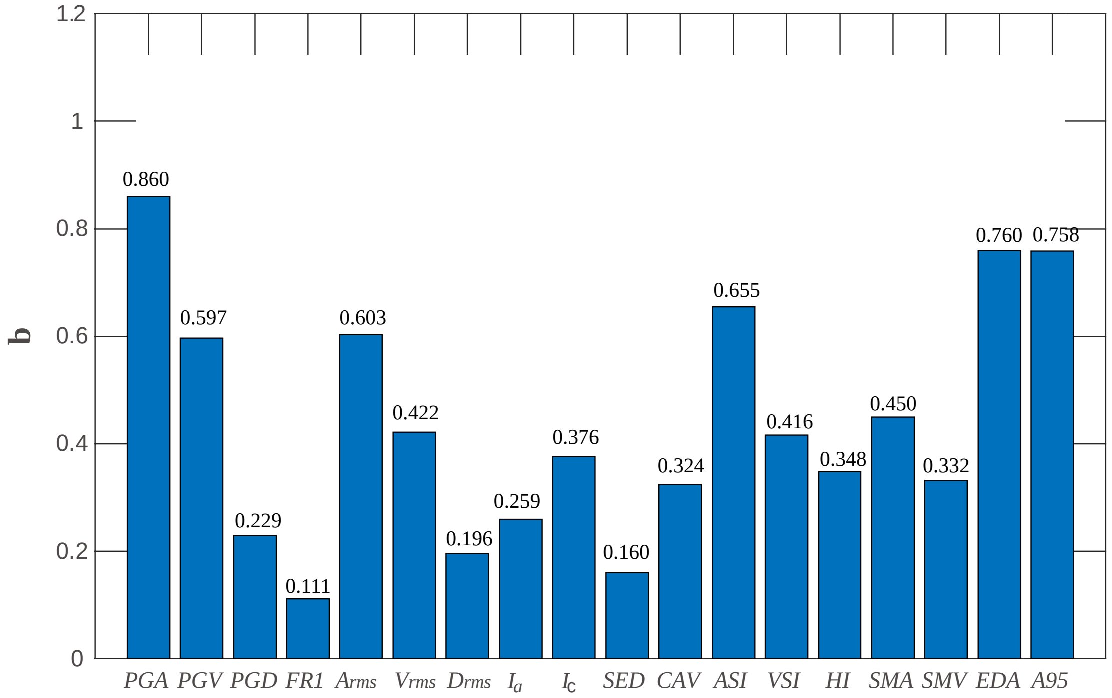

Fig.14. Regression parameter *b* for the 18 tested *IMs* based on the numerical analyses of the shallow tunnel cases

Fig.15 summarises the slopes *b* calculated for all tested *IMs* for the moderately deep tunnel cases. *EDA* is identified as the most practical *IM*, with the three most practical *IMs* being *EDA* > A95 > *PGA*. Their corresponding slopes *b* are 0.739, 0.715, and 0.700, respectively. On the contrary, *SED* exhibits the lowest slope *b* among the others, while the second and third lowest slopes *b* are reported for I_A and D_{rms}, respectively. The slopes *b* for these three least practical *IMs*, i.e. *SED*, I_A, and D_{rms}, are equal to 0.239, 0.290, and 0.355, respectively.

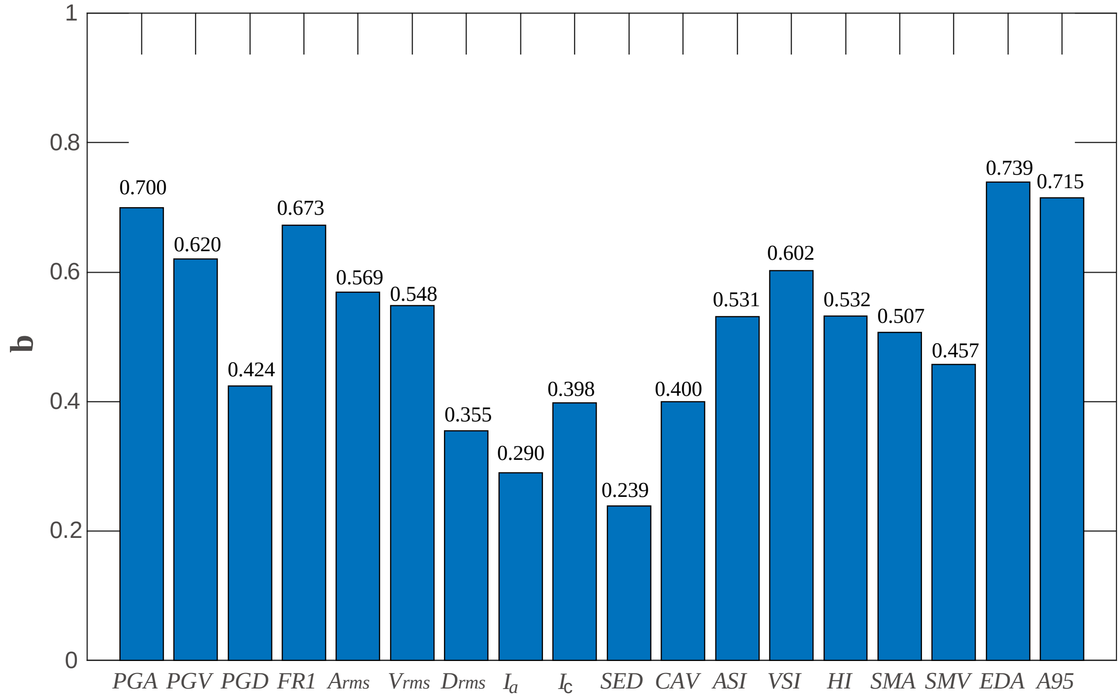

Fig.15. Regression parameter *b* for the 18 tested *IMs* based on the numerical analyses of the moderately deep tunnel cases

For deep tunnels, *FR*1 turns out to be the most practical *IM*, followed by *EDA* and *PGA* (Fig.16) The corresponding slopes *b* are 0.758, 0.735, and 0.711, respectively. *SED* again proves to be the least practical *IM*, because the slope *b* is equal to 0.266. The second and third least practical *IMs* are I_A and D_{rms}, with slopes *b* of 0.313 and 0.399, respectively. Similar results for the least practical *IMs* are also reported for the cases of moderately deep tunnels.

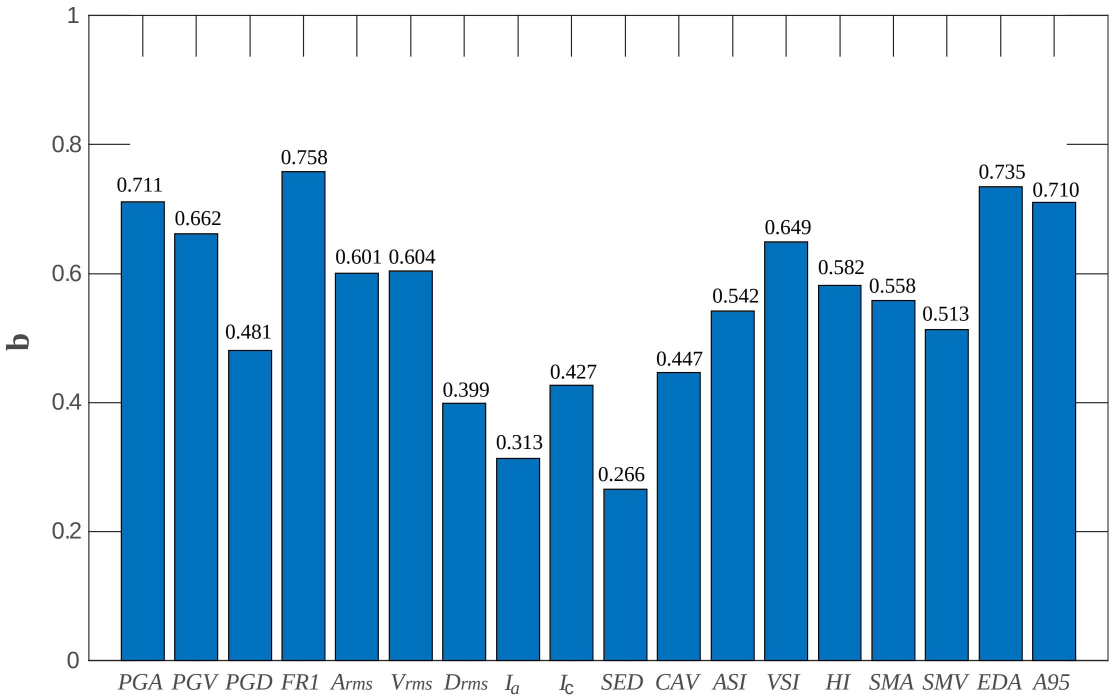

Fig.16. Regression parameter *b* for the 18 tested *IMs* based on the numerical analyses of the deep tunnel cases

3.4.5 Proficiency testing

Proficiency ζ describes the composite effect of practicality and efficiency and was first proposed by Padgett et al. (2008). It is defined according to Eq.(6). Typically, a lower proficiency ζ indicates that using the *IM* introduces less uncertainty into the analysis, i.e., the corresponding *IM* is more proficient.

$$\zeta = \frac{\beta_{\mathrm{D|IM}}}{b} \tag{6}$$

Figs.17–19 compare the computed ζ for the considered *DM* with regard to the 18 tested *IMs* for the shallow, moderately deep, and deep tunnel cases, respectively.

For the shallow tunnel, *PGA* is the most proficient *IM* due to the corresponding smallest ζ of 0.216, followed by *PGV* and *EDA* (Fig.17), which have ζ values of 0.367 and 0.387, respectively, which are quite close to the value for *PGA*. *FR*1 is the less proficient measure, as it has the maximum ζ, i.e. 4.432. The next two least proficient *IMs* are *SED* and D_{rms}. Their corresponding values of ζ are 2.556 and 2.311, respectively, which are considerably lower than the value for *FR*1.

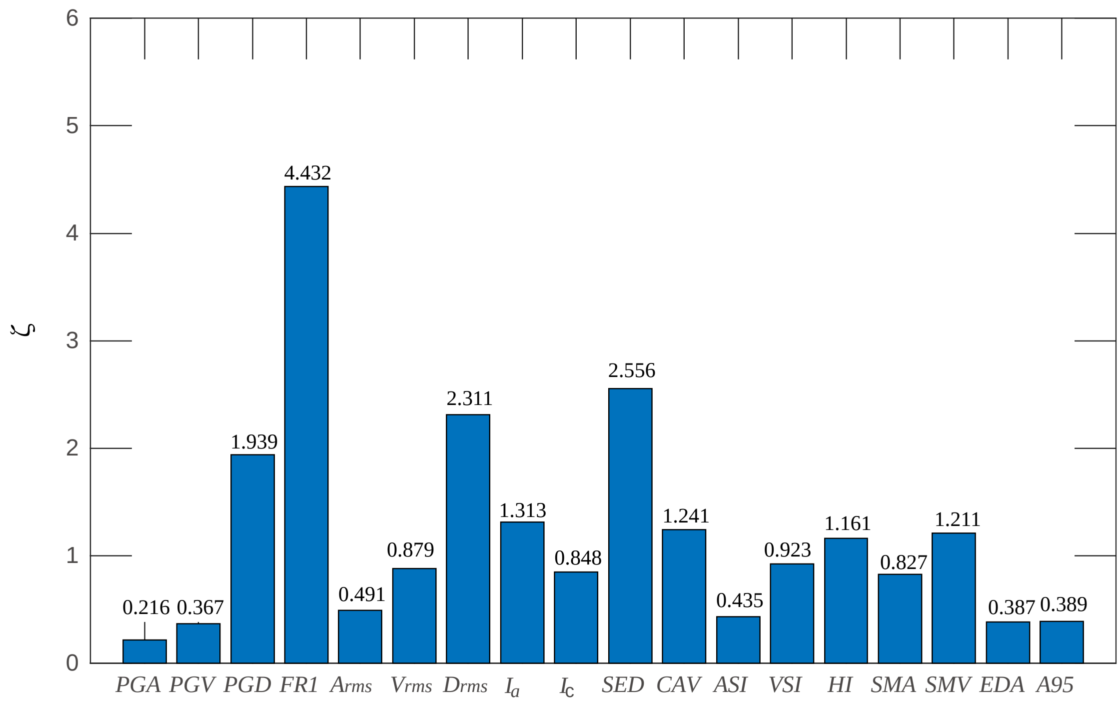

Fig.17. Regression parameter ζ for the 18 tested *IMs* based on the numerical analyses of the shallow tunnel cases

Fig.18 shows the calculated ζ for the moderately deep tunnel cases. For this case, it can be concluded that *PGV* is the most proficient *IM* indicated by the smallest ζ of 0.218 compared to other tested *IMs*. Furthermore, *VSI* and *HI* are two of the other proficient *IMs* with ζ values of 0.272 and 0.368, respectively. *SED* is the least proficient *IM*, followed by D_{rms} and I_A

with corresponding ζ values of 0.996, 0.932, and 0.910, respectively.

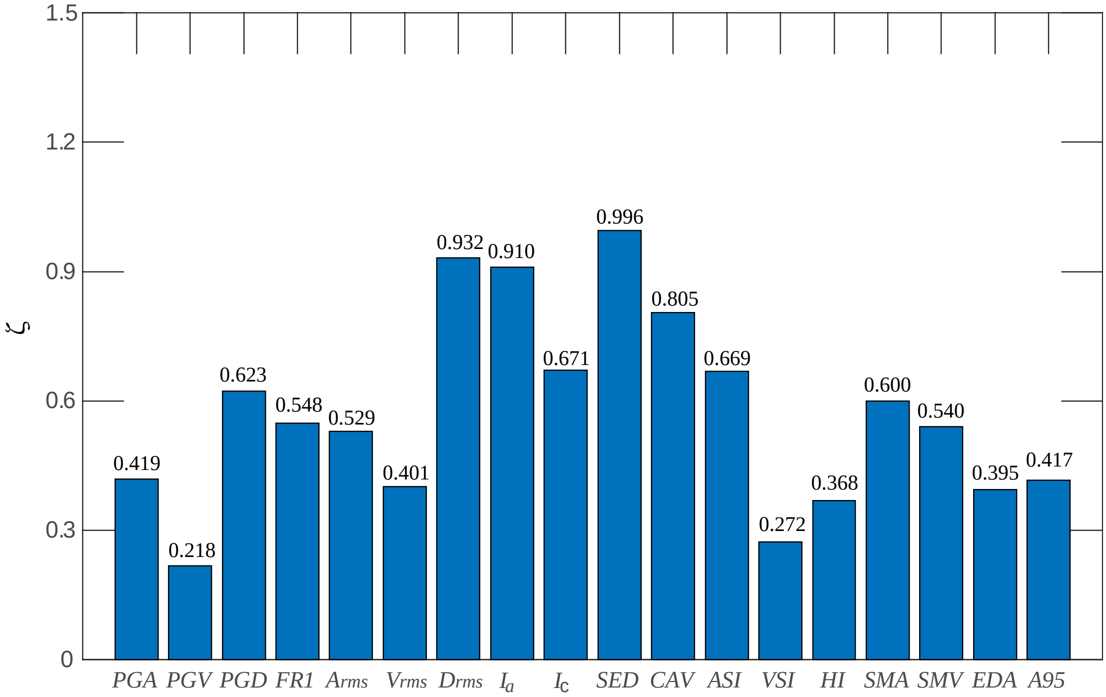

Fig.18. Regression parameter ζ for the 18 tested *IMs* based on the numerical analyses of the moderately deep tunnel cases

Finally, for deep tunnels (Fig.19), *PGV* tends again to be the most proficient *IM*, followed by *VSI* and *HI*. Their corresponding ζ are equal to 0.261, 0.300 and 0.366, respectively. Interestingly, the above observation is also reported for the moderately deep tunnel cases. On the contrary, I_A is found to be the less proficient measure having the highest ζ of 0.952 among all other tested *IMs*. *SED* and D_{rms} are found to be the next two least proficient *IMs* with slightly lower ζ of 0.925 and 0.850, respectively.

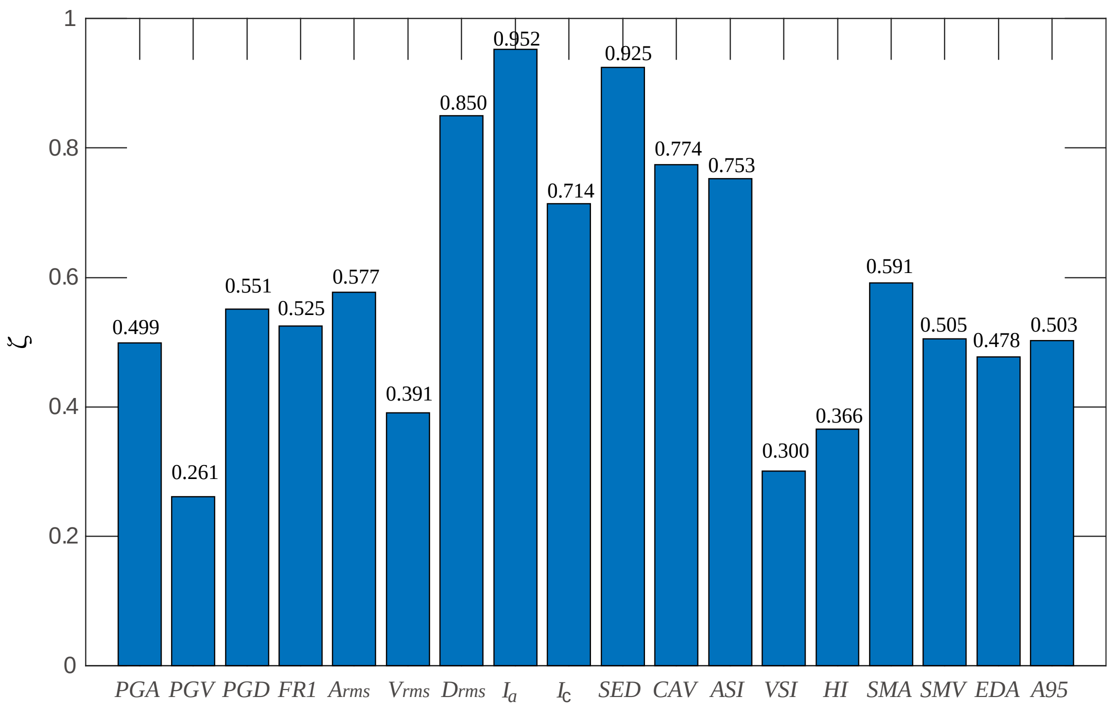

Fig.19. Regression parameter ζ for the 18 tested *IMs* based on the numerical analyses of the deep tunnel cases

3.4.6 Optimal *IM* selections

Table 6 summarises the three most correlated, efficient, practical and proficient *IMs* for shallow, moderately, and deep tunnel cases, based on the above tests. It can be observed that for shallow tunnels, *PGA* is the optimal *IM*, followed by *PGV* and *ASI* or A95. These results are in line with the recent work of Zhong et al. (2020), who also reported that *PGA* is the optimal *IM* for shallow underground structures in the case of Dakai station in Japan. Moreover, *PGV* is identified as the optimal *IM* for both moderately deep and deep tunnels, followed by *VSI* and *HI*. This observation is consistent with some existing works, which reported that *PGV* has better correlation with seismic response of deep underground structures [24, 39]. The above observations highlight the significant role of tunnel burial depth in the selection of *IM* for fragility curve construction. When various tunnel burial depths are considered, *PGV* could be adopted as the unique optimal *IM* at a preliminary stage of quantitative risk analysis. However, it should be noted that *PGA* is still the most widely used *IM* to generate fragility curves for both aboveground structures [76-78] and underground structures [21, 23, 26].

Table 6. Three most correlated, efficient, practicable and proficient *IMs* for shallow, moderately deep, and deep tunnels

Testing criteria	Shallow tunnel			Moderately deep tunnel			Deep tunnel		
	IM								
	1st	2nd	3rd	1st	2nd	3rd	1st	2nd	3rd
Correlation	*PGA*	*PGV*	*ASI*	*PGV*	*VSI*	*HI*	*PGV*	*VSI*	*HI*
Efficiency	*PGA*	*PGV*	*ASI*	*PGV*	*VSI*	*HI*	*PGV*	*VSI*	*HI*
Practicality	*PGA*	*EDA*	*A95*	*EDA*	*A95*	*PGA*	*FR1*	*EDA*	*A95*
Proficiency	*PGA*	*PGV*	*A95*	*PGV*	*VSI*	*HI*	*PGV*	*VSI*	*HI*

4. **Proposed fragility curves**

Based on the PSDM results (Fig. 7) and the selection of the optimal *IM* (Table 6), seismic fragility curves are proposed for shallow, moderately deep, and deep tunnels in terms of minor, moderate, and extensive damage states. Fig.20 depicts the computed analytical fragility curves of the examined circular tunnels with respect to *PGA* or *PGV* at the ground free-field conditions. The parameters of the fragility functions in terms of median IM_{mi} (*PGA* or *PGV*) and standard deviations β_{tot} for circular tunnels in soil type D are listed in Table 7 for the three damage states. Note that the final variability of each fragility curve is described by the total lognormal standard deviation β_{tot} [12], which is modelled by combining three primary sources of uncertainty, as shown in Eq.7:

$$\beta_{tot} = \sqrt{\beta_{ds}^2 + \beta_C^2 + \beta_{\mathrm{D|IM}}^2} \quad (7)$$

where β_{ds} is the uncertainty related to the definition of damage state, *ds*, β_C is the uncertainty related to the response and resistance (seismic capacity) of the element, and $\beta_{\mathrm{D|IM}}$ is the uncertainty from the earthquake input motion (seismic demand). The parameter $\beta_{\mathrm{D|IM}}$ represents the variability in the response of the investigated structure due to the variability of the ground motion and is estimated as the dispersion of the simulated *DMs* with respect to the regression fit for the calculated damage data. The parameters β_{ds} and β_C are considered as 0.4 and 0.3, respectively [25]. The treatment of uncertainties in the fragility analysis is a central issue and the determination of β_{ds} and β_C is challenging. Variable values of β_{ds} and β_C have been adopted for different geotechnical components [13, 79]. To the best of the authors' knowledge, the uncertainty in the threshold value of the damage states β_{ds} and in the capacity β_C of tunnels has not been studied in detail thus far and, hence, further research is needed by employing experimental and monitoring data [80]. The value of β_{ds} is typically ranging between 0.20 and 0.71 [13], while an average value of 0.4 is usually adopted for tunnels [13, 14, 25-35]. Furthermore, the uncertainty in the capacity β_C is commonly between 0.14 and 0.50 [13], whereas a value of 0.3 is usually assumed based on engineering judgment for tunnels [13, 14, 25-35]. In this paper, the adopted values of β_{ds} and β_C are consistent with previous similar studies [25-35] due to the absence of relevant studies and a more rigorous estimation. A more detailed introduction on the treatment of uncertainties for the fragility curves of tunnels and other underground structures can also be found in Argyroudis et al. [13], Selva et al. [79] and Huang et al. [14].

The case of shallow tunnel is used in this study to evaluate the influence of the values of β_{ds} and β_C on the total standard deviation β_{tot} and finally on the resulting fragility curves. The uncertainty in the demand $\beta_{\mathrm{D|IM}}$ is equal to 0.186 for shallow tunnels. Hence, based on Eq.7, a total standard deviation β_{tot}, between 0.307 and 0.888 is calculated, when the aforementioned range of β_{ds} and β_C values is considered. The average value of β_{tot} in this case is equal to 0.597, which is close to the corresponding value in Table 7, i.e. 0.533. Moreover, a higher value for β_{ds} and β_C would increase β_{tot}, resulting in a larger slope of the fragility curves. For example, an increase of 0.1 for β_{ds} and β_C would increase the values of β_{tot} in Table 7 to 0.667 for the shallow tunnel case, which corresponds to an average increase of 1.8% in the slope of the fragility curves for minor damage state. The opposite effect is expected when lower values of β_{ds} and β_C were assumed, i.e., decrease in the slope of the fragility curves. Similar conclusions can be drawn for the moderately deep and deep tunnels.

The fragility curves developed in this study can be applied to assess the seismic vulnerability of circular tunnels in similar soft soil deposits. For instance, for the shallow circular tunnels located in Shanghai, China, the design ground acceleration for an exceedance probability of 10% in 50 years according to the Code for Seismic Design of Buildings [61] is 0.10 g and 0.20 g, respectively. For *PGA*=0.10 g, the probability of exceeding minor damage is equal to 1.0%, whereas the probabilities of exceeding moderate and extensive damage are negligible. When the *PGA* increases to 0.20 g, the probability of minor damage increases to 14.9%, while the probabilities of moderate and extensive damage increase slightly but are still very small. These results show that the studied tunnels can maintain their basic performance but suffer some minor damage under these earthquake intensities.

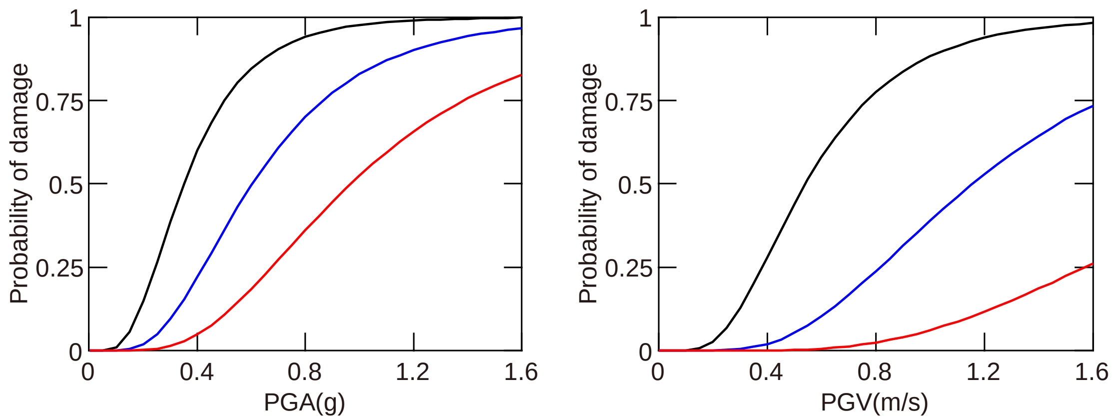

(a) Shallow tunnel **(b) Moderately deep tunnel**

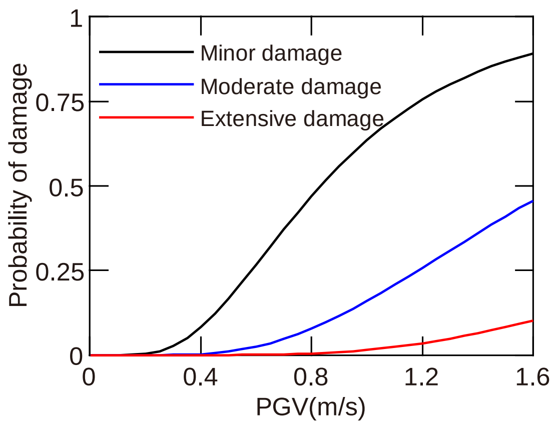

(c) Deep tunnel

Fig.20. Fragility curves for shallow, moderately deep and deep tunnels

Table 7. Derived parameters of the fragility curves in terms of *PGA* or *PGV* at free-field ground surface for circular tunnel with various burial depths in soil type D

Damage states	Minor	Moderate	Extensive	β_{tot}
Shallow tunnel (*h* = 9 m)	0.350 (g)	0.604 (g)	0.968 (g)	0.533
Moderately deep tunnel (*h* = 20 m)	0.542 (m/s)	1.156 (m/s)	2.225 (m/s)	0.518
Deep tunnel (*h* = 30 m)	0.833 (m/s)	1.694 (m/s)	3.124 (m/s)	0.529

5. Conclusions

In this work, different seismic *IMs* are tested to identify the optimal ones for the development of PSDMs for circular tunnels embedded in soft soil deposits, when subjected to transverse seismic excitation. Critical parameters affecting the seismic response of tunnels, including soil conditions, tunnel burial depth, and ground motion characteristics, were thoroughly considered. The tunnel lining response under ground shaking was evaluated using 2D nonlinear dynamic analyses, for gradually increasing seismic intensity. The *DM* was defined based on the exceedance of the bending moment capacity of the tunnel lining, while the values of the selected *IMs* were generated from the free-field ground surface for each analysed case. The selected *IMs* were tested using the correlation, efficiency, practicality, and proficiency metrics, with the aim of identifying the optimal *IMs* from the selected ones for the examined soil-tunnel systems. The significant effect of tunnel burial depths on the selection of optimal *IMs* was highlighted. The results indicated that *PGA* was the optimal *IM* for shallow tunnels, followed by *PGV* and *ASI* or *A95*. Moreover, *PGV* was found to be the optimal *IM* for moderately deep and deep tunnels, followed by *VSI* and *HI*. This observation highlights that *PGA*, the most commonly used metric, is not always the best *IM* for seismic fragility analysis of tunnels. Finally, the proposed optimal *IMs* were adopted to generate seismic fragility curves of circular tunnels embedded in soft soil deposits. The study provides a guide for more accurate and reliable performance-based assessment of seismic risk and resilience of circular tunnels embedded in soft soil deposits. The findings can be used in future studies as a basis for investigating the effects of other tunnel typologies, soil conditions, or damage measures, and for selecting the optimal *IM* for seismic fragility analysis of tunnels and underground infrastructure. Future research can consider the effect of the tunnel excavation process, examine alternative damage measures for the derivation of analytical fragility curves, and investigate the uncertainties in the capacity and definition of limit states based on experimental studies and monitoring data.

Acknowledgements

This work is substantially supported by National Natural Science Foundation of China (under grants No. 52090082, 41772295, 51978517), Innovation Program of Shanghai Municipal Education Commission (under grant No. 2019-01-07-00-07-456 E00051) and key innovation team program of innovation talents promotion plan by MOST of China (under No. 2016RA4059). The support is gratefully acknowledged. The first author also wishes to thank Professor Kyriazis Pitilakis and Professor Dong-Mei Zhang for their supervisions for this research. This study has been conducted in the Laboratory of Soil Dynamics and Geotechnical

Earthquake Engineering of Aristotle University, Thessaloniki, Greece.

References

[1] Zhang DM, Huang ZK, Li ZL, Zong X, Zhang DM, Analytical solution for the response of an existing tunnel to a new tunnel excavation underneath. Comput. Geotech. 2019;108:197-211.

[2] Zhang DM, Huang ZK, Yin ZY, Ran RZ, Huang HW, Predicting the grouting effect on leakage-induced tunnels and ground response in saturated soils. Tunn. Undergr. Space Technol. 2017; 65:76-90.

[3] Tsinidis G, de Silva F, Anastasopoulos I, et al. Seismic behaviour of tunnels: From experiments to analysis. Tunn. Undergr. Space Technol. 2020;99: 103334.

[4] Hatzigeorgiou GD, Beskos DE. Soil-structure interaction effects on seismic inelastic analysis of 3-D tunnels. Soil Dynam Earthquake Engng 2010; 30(9):851-861.

[5] Pitilakis K, Tsinidis G. Performance and seismic design of underground structures.Earthquake geotechnical engineering design. Springer, Cham, 2014;pp: 279-340.

[6] Iida H, Hiroto T, Yoshida N, et al. Damage to Daikai subway station[J]. Soils Found. 1996; 36(Special): 283-300.

[7] Parra-Montesinos GJ, Bobet A, Ramirez JA. Evaluation of soil-structure interaction and structural collapse in Daikai subway station during Kobe earthquake[J]. ACI Struct. J. 2006; 103(1): 113.

[8] O Rourke TD, Goh SH, Menkiti CO, et al. Highway tunnel

performance during the 1999 Duzce earthquake. Proceedings of the international conference on soil mechanics and geotechnical engineering. AA BALKEMA PUBLISHERS, 2002;2: 1365-1368.

[9] Kontoe S, Zdravkovic L, Potts D M, et al. Case study on seismic tunnel response. Can. Geotech. J. 2008;45(12): 1743-1764.

[10] Wang ZZ, Zhang Z. Seismic damage classification and risk assessment of mountain tunnels with a validation for the 2008 Wenchuan earthquake. Soil Dyn. Earthq. Eng. 2013;45: 45-55.

[11] Yu H, Chen J, Bobet A, et al. Damage observation and assessment of the Longxi tunnel during the Wenchuan earthquake. Tunn. Undergr. Space Technol. 2016; 54: 102-116.

[12] Pitilakis K, Crowley H, Kaynia A M. SYNER-G: typology definition and fragility functions for physical elements at seismic risk. Geotechnical, Geological and Earthquake Engineering, 2014; 27: 1-28.

[13] Argyroudis S A, Mitoulis S A, Winter M G, et al. Fragility of transport assets exposed to multiple hazards: State-of-the-art review toward infrastructural resilience. Reliab. Eng. Syst. Saf. 2019; 191: 106567.

[14] Huang ZK, Pitilakis K, Tsinidis G, et al. Seismic vulnerability of circular tunnels in soft soil deposits: The case of Shanghai metropolitan system. Tunn. Undergr. Space Technol. 2020; 98:

103341.

[15] Giovenale P, Cornell C A, Esteva L. Comparing the adequacy of alternative ground motion intensity measures for the estimation of structural responses.Earthq. Eng. Struct. Dyn. 2004;33(8): 951-979.

[16] Padgett J E, Nielson B G, DesRoches R. Selection of optimal intensity measures in probabilistic seismic demand models of highway bridge portfolios. Earthq. Eng. Struct. Dyn. 2008; 37(5): 711-725.

[17] Housner GW, Spectrum intensities of strong motion earthquakes. Proceedings of symposium of earthquake and blast effects on structures, EERI, Los Angeles, California. 1952; 21–36.

[18] Mackie K, Stojadinović B. Probabilistic seismic demand model for California highway bridges. J. Bridge Eng. 2001; 6(6): 468-481.

[19] Avanaki MJ, Hoseini A, Vahdani S, et al. Seismic fragility curves for vulnerability assessment of steel fiber reinforced concrete segmental tunnel linings. Tunn. Undergr. Space Technol. 2018; 78: 259-274.

[20] Wang X, Shafieezadeh A, Ye A. Optimal intensity measures for probabilistic seismic demand modeling of extended pile-shaft-supported bridges in liquefied and laterally spreading ground. Bull. Earthq. Eng. 2018;16(1): 229-257.

[21] ATC-13, Earthquake Damage Evaluation Data for California,

Applied Technology Council, Redwood City. 1985.
[22] ALA, Seismic Fragility Formulations for Water Systems: Part 1-Guideline. American Society of Civil Engineers-FEMA. 2001.
[23] HAZUS, Multi-Hazard Loss Estimation Methodology: Earthquake Model. Department of Homeland Security, FEMA, Washington, DC, USA. 2004.
[24] Corigliano M, Lai C G, Barla G. Seismic vulnerability of rock tunnels using fragility curves. 11th ISRM Congress, Lisbon, Portugal. International Society for Rock Mechanics. 2007.
[25] Argyroudis SA, Pitilakis KD. Seismic fragility curves of shallow tunnels in alluvial deposits. Soil Dyn. Earthq. Eng. 2012; 35: 1-12.
[26] Argyroudis S, Tsinidis G, Gatti F, et al. Effects of SSI and lining corrosion on the seismic vulnerability of shallow circular tunnels. Soil Dyn. Earthq. Eng. 2017; 98: 244-256.
[27] Huang G, Qiu W, Zhang J. Modelling seismic fragility of a rock mountain tunnel based on support vector machine. Soil Dyn. Earthq. Eng. 2017;102:160–171.
[28] Qiu W, Huang G, Zhou H, et al. Seismic vulnerability analysis of rock mountain tunnel. Int. J. Geomech. 2018;18:04018002.
[29] de Silva F, Fabozzi S, Nikitas N, et al., Site Specific Seismic Performance of Circular Tunnels in Dry Sand. In National Conference of the Researchers of Geotechnical Engineering. Springer, Cham.

2019.

[30] de Silva F, Fabozzi S, Nikitas N, et al. Seismic vulnerability of circular tunnels in sand. Géotechnique, 2020; 1-15.

[31] Hu X, Zhou Z, Chen H, et al. Seismic fragility analysis of tunnels with different buried depths in a soft soil. Sustainability. 2020; 12(3): 892.

[32] Huh J, Le T S, Kang C, et al. A probabilistic fragility evaluation method of a RC box tunnel subjected to earthquake loadings. J. Korean Tunn. Undergr. Space Assoc. 2017; 19(2): 143-159.

[33] Huh J, Tran Q H, Haldar A, et al. Seismic vulnerability assessment of a shallow two-story underground RC box structure. Appl. Sci. 2017; 7(7): 735.

[34] Nguyen DD, Park D, Shamsher S, et al. Seismic vulnerability assessment of rectangular cut-and-cover subway tunnels. Tunn. Undergr. Space Technol. 2019; 86: 247-261.

[35] Mayoral J M, Argyroudis S, Castañon E. Vulnerability of floating tunnel shafts for increasing earthquake loading. Soil Dyn. Earthq. Eng. 2016;80: 1-10.

[36] Liu T, Chen ZY, Yuan Y, Shao XY, Fragility analysis of a subway station structure by incremental dynamic analysis. Adv. Struct. Eng. 2016;20 : 1111–1124.

[37] Andreotti G, Lai C, Use of fragility curves to assess the seismic

vulnerability in the risk analysis of mountain tunnels. Tunn. Undergr. Space Technol.2019; 91:103008.

[38] Zhong ZL, Shen Y, Zhao M, Li L, Du XL, Hao H, Seismic fragility assessment of the Daikai subway station in layered soil. Soil Dyn. Earthq. Eng. 2020;132:106044.

[39] Chen ZY, Wei J, Correlation between ground motion parameters and lining damage indices for mountain tunnels. Nat. Hazards. 2013;65:1683–1702.

[40] Luco N, Cornell CA, Structure-specific scalar intensity measures for near-source and ordinary earthquake ground motions. Earthq. Spectra.2007; 23:357-392.

[41] Shome N, Cornell CA, Probabilistic Seismic Demand Analysis of Nonlinear Structures. Report no. RMS-35. Stanford, CA: RMS Program, Stanford University. 1999.

[42] Elenas A, Meskouris K, Correlation study between seismic acceleration parameters and damage indices of structures. Eng. Struct. 2001;23: 698-704.

[43] Pejovic JR, Serdar NN, Pejovic RR, Optimal intensity measures for probabilistic seismic demand models of RC high-rise buildings. Earthq. Struct. 2017;13:221-230.

[44] Nguyen DD, Thusa B, Han TS, Lee TH, Identifying significant earthquake intensity measures for evaluating seismic damage and

fragility of nuclear power plant structures. Nucl. Eng. Technol. 2020; 52:192-205.

[45] Shafieezadeh A, Ramanathan K, Padgett JE, DesRoches R, Fractional order intensity measures for probabilistic seismic demand modeling applied to highway bridges. Earthq. Eng. Struct. Dyn. 2012;41: 391-409.

[46] Guo J, Alam MS, Wang J, Li S, Yuan W, Optimal intensity measures for probabilistic seismic demand models of a cable-stayed bridge based on generalized linear regression models. Soil Dyn. Earthq. Eng. 2020; 131:106024.

[47] Shakib H, Jahangiri V, Intensity measures for the assessment of the seismic response of buried steel pipelines. Bull. Earthq. Eng. 2016;14:1265-1284.

[48] Hariri-Ardebili MA, Saouma VE, Probabilistic seismic demand model and optimal intensity measure for concrete dams. Struct. Saf. 2016;59: 67-85.

[49] ABAQUS, ABAQUS: Theory and analysis user’s manual, version 6.12. Dassault Systèmes SIMULIA, Providence, RI, USA. 2012.

[50] Tsinidis G, Pitilakis K, Madabhushi G, Heron C, Dynamic response of flexible square tunnels: centrifuge testing and validation of existing design methodologies. Geotechnique. 2015; 65:401–417.

[51] Lysmer J, Kuhlemeyer RL, Finite dynamic model for infinite

media. J Eng. Mech. D ASCE. 1969;95: 859–878.

[52] Bardet JB, Ichii K, Lin CH, EERA: A Computer Program for Equivalent-linear Earthquake Site Response Analyses of Layered Soil Deposits. University of Southern California, Department of Civil Engineering, Los Angeles. 2000.

[53] FHWA (Federal Highway Administration), Technical manual for design and construction of road tunnels-Civil elements. Publication No. FHWA-NHI-10-034. Department of transportation, Federal Highway Administration, Washington D.C., U.S. 2009.

[54] Cilingir U, Madabhushi SPG, Effect of depth on the seismic response of circular tunnels. Can. Geotech. J.2010; 48:117–127.

[55] Cilingir U, Madabhushi SPG, A model study on the effects of input motion on the seismic behavior of tunnels. Soil Dyn. Earthq. Eng. 2011; 31:452–462.

[56] Hashash YM, Park D, Viscous damping formulation and high frequency motion propagation in non-linear site response analysis. Soil Dyn. Earthq. Eng.2002; 22:611-624.

[57] Vamvatsikos D, Cornell CA, Incremental dynamic analysis. Earthquake Eng. Struct. Dyn. 2002;31:491-514.

[58] Gelagoti F, Kourkoulis R, Anastasopoulos I, Gazetas G, Rocking isolation of low-rise frame structures founded on isolated footings. Earthq. Eng. Struct. Dyn. 2012;41:1177–1197.

[59] EC8, Eurocode 8: Design of Structures for Earthquake Resistance. The European Standard EN 1998-1, Brussels, Belgium. 2004.

[60] GB50011, Code for Seismic Design of Buildings. China Architecture and Building Press, Beijing, China. 2010. (in Chinese)

[61] DG/TJ08-2064-2009, Code for Seismic Design of Subway Structures, Shanghai Urban Constructions Communications, Shanghai, China. 2010. (in Chinese)

[62] Iervolino I, Manfredi G, A review of ground motion record selection strategies for dynamic structural analysis. In Modern Testing Techniques for Structural Systems. Springer, Vienna. 2008; 131-163.

[63] Pacific Earthquake Engineering Research Center (PEER), PEER Strong Motion Database. Berkeley, CA: University of California, Berkeley. 2000.

[64] Kramer SL, Geotechnical earthquake engineering. Pearson Education India. 1996.

[65] Housner GW, Jennings PC, Generation of artificial earthquakes. J. Eng. Mechanics Division, ASCE 90 (EM1). 1964; 113–150.

[66] Arias A, A measure of earthquake intensity. Seismic Design for Nuclear Power Plants. Massachusetts Institute of Technology. 1970.

[67] Park YJ, Alfredo HS, Wen YK. Seismic damage analysis of reinforced concrete buildings. J. Str. Eng. 1985;111: 740-757.

[68] Nuttli OW, The relation of sustained maximum ground

acceleration and velocity to earthquake intensity and magnitude. US Army Engineer Waterways Experiment Station. 1979.

[69] Benjamin JR, A criterion for determining exceedances of the operating basis earthquake, Epri report np-5930. Electric Power Research Institute, Palo Alto. 1988.

[70] Sarma SK, Yang KS. An evaluation of strong motion records and a new parameter A95. Earthq. Eng. Struct. Dyn. 1987;15(1): 119-132.

[71] Cornell C A, Jalayer F, Hamburger R O, et al. Probabilistic basis for 2000 SAC federal emergency management agency steel moment frame guidelines. J. Struct. Eng. 2002; 128(4): 526-533.

[72] Zampieri P, Zanini M A, Faleschini F. Derivation of analytical seismic fragility functions for common masonry bridge types: methodology and application to real cases. Eng. Fail. Anal. 2016;68: 275-291.

[73] Zareei S A, Hosseini M, Ghafory-Ashtiany M. Seismic failure probability of a 400 kV power transformer using analytical fragility curves. Eng. Fail. Anal. 2016; 70: 273-289.

[74] Mosoarca M, Onescu I, Onescu E, et al. Seismic vulnerability assessment methodology for historic masonry buildings in the near-field areas Eng. Fail. Anal. 2020: 104662.

[75] Ozdemir M A, Kaya E S, Aksar B, et al. Seismic vulnerability of masonry Jack arch slabs. Eng. Fail. Anal. 2017; 77: 146-159.

[76] Choi E, DesRoches R, Nielson B. Seismic fragility of typical bridges in moderate seismic zones. Eng. Struct. 2004, 26(2): 187-199.

[77] Ramanathan K, Padgett J E, DesRoches R. Temporal evolution of seismic fragility curves for concrete box-girder bridges in California. Eng. Struct. 2015; 97: 29-46.

[78] Adhikari R, Gautam D. Component level seismic fragility functions and damage probability matrices for Nepali school buildings. Soil Dyn. Earthq. Eng. 2019; 120: 316-319.

[79] Selva J, Argyroudis S, Pitilakis K. Impact on loss/risk assessments of inter-model variability in vulnerability analysis. Nat. hazard. 2013; 67(2): 723-746.

[80] Achillopoulou DV, Mitoulis SA, Argyroudis SA, Wang Y. Monitoring of transport infrastructure exposed to multiple hazards: A roadmap for building resilience. Sci. Total Environ. 2020; 746, 141001.

Table list

Figure list

Fig.1 Schematic of the analytical framework for the fragility analysis of tunnels

Fig.2. 2D numerical model of the soil-tunnel system

Fig.3. Soil properties for the examined soil deposits

Fig.4. Adopted G-γ-D curves for clayey and sandy deposits

Fig.5. Acceleration response spectra of the selected records

Fig.6. Bending moment time histories computed for EQ2 at a crucial lining section (θ=45°) of the tunnel located in soil type D3, (a) shallow tunnel, (b) moderately deep tunnel, and (c) deep tunnel

Fig.7. Regression analyses between 4 representative seismic *IMs* and *DM* (shallow tunnel)

Fig.8. Regression parameter R^2 for the 18 tested *IMs* based on the numerical analyses of the shallow tunnel cases

Fig.9. Regression parameter R^2 for the 18 tested *IMs* based on the numerical analyses of the moderately deep tunnel cases

Fig.10. Regression parameter R^2 for the 18 tested *IMs* based on the numerical analyses of the deep tunnel cases

Fig.11. Regression parameter $\beta_{D/IM}$ for the 18 tested *IMs* based on the numerical analyses of the shallow tunnel cases

Fig.12. Regression parameter $\beta_{D/IM}$ for the 18 tested *IMs* based on the numerical analyses of the moderately deep tunnel cases

Fig.13. Regression parameter $\beta_{D/IM}$ for the 18 tested *IMs* based on the numerical analyses of the moderately deep tunnel cases

Fig.14. Regression parameter *b* or the 18 tested *IMs* based on the numerical analyses of the shallow tunnel cases

Fig.15. Regression parameter *b* for the 18 tested *IMs* based on the numerical analyses of the moderately deep tunnel cases

Fig.16. Regression parameter *b* for the 18 tested *IMs* based on the numerical analyses of the moderately deep tunnel cases

Fig.17. Regression parameter ζ for the 18 tested *IMs* based on the numerical analyses of the shallow tunnel cases

Fig.18. Regression parameter ζ for the 18 tested *IMs* based on the numerical analyses of the moderately deep tunnel cases

Fig.19. Regression parameter ζ for the 18 tested *IMs* based on the numerical analyses of the moderately deep tunnel cases

Fig.20. Fragility curves for shallow, moderately deep and deep tunnels